https://doi.org/10.5194/egusphere-2026-59
Preprint. Discussion started: 28 January 2026

Tracing biological, human, and inorganic sources of coarse aerosols via single-particle fluorescence and optical morphology

Aiden Jönsson[1,2], Jinglan Fu[1,2,3], Gabriel Pereira Freitas[1,2], Ian Crawford[4], Pavla Dagsson-Waldhauserová[5,6], Radovan Krejci[1,2], Yutaka Tobo[7,8], Karl Espen Yttri[9], and Paul Zieger[1,2]

[1]Department of Environmental Science, Stockholm University, Stockholm, Sweden
[2]Bolin Centre for Climate Research, Stockholm University, Stockholm, Sweden
[3]Now at: Centre for Isotope Research, Faculty of Science and Engineering, University of Groningen, Groningen, the Netherlands
[4]Department of Earth and Environmental Science, University of Manchester, Manchester, United Kingdom
[5]Agricultural University of Iceland, Hvanneyri, Iceland
[6]Czech University of Life Sciences, Prague, Czech Republic
[7]National Institute of Polar Research, Tackikawa, Tokyo, Japan
[8]Graduate Institute for Advanced Studies SOKENDAI, Tachikawa, Tokyo, Japan
[9]The Climate and Environmental Research Institute NILU, Kjeller, Norway

Correspondence: A. Jönsson (aiden.jonsson@aces.su.se) and P. Zieger (paul.zieger@aces.su.se)

Abstract.

Coarse-mode aerosol particles influence the environment, climate, and human health in diverse ways depending on their type. While mineral dust and sea spray aerosol (SSA) dominate this size range, rarer biological particles can have outsized impacts, for example by initiating ice formation at relatively warm temperatures. Hence, accurate, type-specific characterization of coarse-mode aerosol is essential for understanding their roles in climate and the environment. Using laboratory measurements of single-particle ultraviolet light-induced fluorescence (UV-LIF) spectroscopy and morphology, we provide a new reference dataset for coarse-mode aerosols from common sources, including pollen, dust, bacteria, and microplastics. Comparisons with previously published datasets reveal consistent source-dependent fluorescence features, but also highlights similarities between biological and non-biological particles that can bias classifications based on fluorescence alone.

We present an improved machine learning-based classification algorithm that integrates fluorescence and morphology using laboratory data for training, and evaluate its performance using observations made at Zeppelin Observatory, Svalbard. We apply domain adaptation using field data to improve the identification of combustion-sourced particles, and to better distinguish dust from SSA. The new algorithm reproduces the previously published annual bioaerosol cycle, yields higher concentrations than a fluorescence-only approach, and maintains comparable correlations with biological and combustion tracers. This open-source algorithm provides a basis for quantifying bioaerosols across diverse environments, can revise bioaerosol estimates in previously analyzed observations, and can be refined as additional characterization data become available.

https://doi.org/10.5194/egusphere-2026-59
Preprint. Discussion started: 28 January 2026

1 Introduction

The chemical and physical properties of aerosol particles determine how they interact with atmospheric radiation and moisture, and thus influence climate and weather. Detailed knowledge about these parameters is therefore important for understanding and predicting their impacts. Among primary coarse-mode (defined as supermicron-scale) aerosols, dust and sea spray aerosols (SSA) dominate the global aerosol mass burden (Choobari et al., 2014; Textor et al., 2006) and contribute substantially to solar radiation extinction (Gliß et al., 2021). Both play key roles in atmospheric processes: mineral dust can nucleate ice and trigger heterogeneous freezing in mixed-phase clouds at temperatures $<$20°C (Murray et al., 2012; Hoose and Möhler, 2012; Adebiyi et al., 2023), whereas SSA provide highly hygroscopic surfaces that facilitate important chemical reactions (Bertram et al., 2018; Schiffer et al., 2018). Primary biological aerosol particles (PBAPs), such as pollen, bacteria, fungal spores, and decomposing biological matter, are important for biology, ecology, and human society as vectors of genetic material and pathogens; however, they can also influence climate. In the atmosphere, PBAPs can nucleate ice at much warmer temperatures than dust, with some airborne bacteria being capable of initiating freezing at temperatures as high as -2°C (Maki et al., 1974). Although PBAPs are far less abundant and highly variable, typically between 10^{-3}-10^{1} L^{-1}, even low concentrations in mixed-phase clouds may substantially affect cloud properties due to highly efficient glaciation feedbacks (Huang et al., 2021).

Attaining robust information on aerosol type, provenance, and composition is not trivial. Offline analysis can offer valuable information about aerosol type, but it is labor-intensive, placing limitations on sampling. Online aerosol mass spectrometry offers higher time resolution for chemical composition, but it can typically resolve only one size range per instrument (Nash et al., 2006; Pratt and Prather, 2012). Single-particle mass spectrometry can offer valuable, highly resolved particle composition information, but has highly size-dependent, low ($\ll$50%) detection efficiencies (e.g. Jacquot et al. 2024) and is costly and difficult to miniaturize, making its employment quite rare (Lai et al., 2025). Similarly, quantifying PBAP concentrations with offline methods generally requires labor-intensive analysis using e.g. flow cytometry or microscopy (Després et al., 2012).

Fluorescence is a composition-dependent phenomenon that can provide information about particle type. It has long been implemented in offline analytical methods and, more recently, in online particle detectors. Fluorescence refers to the relaxation of electronically excited molecules by emitting photons in the visible range after excitation by absorbing light, usually in the ultraviolet (UV) or (less commonly) visible spectrum. The emitted light has a longer wavelength than the excitation light (Fu and Finney, 2018). Fluorophores, such as the amino acid tryptophan and coenzymes such as riboflavin, are common in biological material; thus, bioaerosols often fluoresce strongly (Pöhlker et al., 2012).

In UV light-induced fluorescence (UV-LIF) techniques, sampled particles are exposed to UV light and their visible fluorescence is measured in order to detect fluorophores. UV-LIF spectroscopy additionally resolves the fluorescence emission's spectral dependence, providing proxy information for particle composition at high sampling resolution. This technique has been implemented in several single-particle bioaerosol detectors, including the Wideband Integrated Bioaerosol Sensor (WIBS; Droplet Measurement Technologies, LLC, USA), UV Aerodynamic Particle Sizer (UVAPS; TSI Inc., USA), SwisensPoleno bioaerosol monitor (Swisens AG, Switzerland; Sauvageat et al. 2020), Real-time Airborne Particle Identifier (RAPID; Plair SA, Switzerland; Sikoparija et al. 2024), and Multiparameter Bioaerosol Spectrometer (MBS; University of Hertfordshire,

https://doi.org/10.5194/egusphere-2026-59
Preprint. Discussion started: 28 January 2026

UK; Ruske et al. 2017). Many of these instruments target the fluorescence of proteins such as tryptophan (excited at 280 nm), while some use multiple excitation wavelengths to probe for a wider range of fluorophores (Pöhlker et al., 2012). Besides PBAPs, biogenic compounds, including fluorophores, can occasionally be present in dust and SSA, potentially influencing atmospheric processes such as ice nucleation (Tobo et al., 2014; Conen and Yakutin, 2018; Wolf et al., 2020; Hartmann et al., 2025). Most UV-LIF instruments also measure optical properties that describe particle morphology, which can be combined with fluorescence spectra for particle characterization. Although fluorescence is not an exact or quantitative technique for determining composition, these instruments provide ample information with which to identify and quantify PBAPs.

A key challenge is that fluorophores are also common in non-biological particles, posing potential problems for PBAP identification. Polycyclic aromatic hydrocarbons (PAHs) are highly fluorescent (Zhang et al., 2017) and are emitted by the combustion of biomass and fossil fuels. PAHs can also coat co-emitted soot and other non-biological particles, causing them to fluoresce (e.g. Toprak and Schnaiter 2013; Yu et al. 2016). Plastic polymers may contain trace amounts of PAHs from production and thus fluoresce, a property used to detect airborne and marine microplastics (Morgana et al., 2024; Gratzl et al., 2024; Pandey et al., 2022). Although the primary target of the instruments listed above is bioaerosol detection, identifying and quantifying particles of anthropogenic origin may also be a useful application for UV-LIF methods in environmental science.

In this study, we characterized coarse-mode particles from climate-relevant sources and likely interferents in the laboratory to build a reference dataset and improve ambient detection. Fluorescence and morphology measurements were made using the MBS, a single-particle UV-LIF spectrometer that also measures optical scattering properties (Section 3.1). We compared our results with published laboratory datasets (Section 3.2) and assessed the implications for particle identification, and built a generalized machine learning (ML) particle classification algorithm trained on these data (Section 3.3). Finally, we applied the algorithm to field observations made with the MBS at the Zeppelin Observatory at Svalbard and validated its performance against parallel measurements of relevant tracer species and PBAP estimates from a previously used decision-tree particle classifier based solely on fluorescence (Section 3.4).

2 Methods and materials

2.1 The multiparameter bioaerosol spectrometer

We use a Multiparameter Bioaerosol Spectrometer (MBS; University of Herefordshire, UK), a UV-LIF spectroscopy device developed for detecting bioaerosols in ambient air (Ruske et al., 2017). The MBS operates at an adjustable fixed instrument flow rate, typically between 1-2.5 L min^{-1}, but particle measurement frequency is constrained by coded triggering sequences. A fixed fraction of the total flow (0.165) is drawn as sample flow with the remainder serving as sheath flow. In the measurement stage, each particle passes sequentially through a low-power laser beam for sizing and a high-power pulsed laser beam for diffraction pattern measurement and is then exposed to a Xenon flash lamp emitting 280 nm to excite fluorescence. Light scattered from the sizing laser is detected using a photomultiplier, and the particle's size is estimated using Mie scattering theory. The high-power laser emits a 10 µs pulse of light for each particle; light scattered by the particle is directed through a beam splitter to two 512-pixel complementary metal oxide semiconductor (CMOS) arrays positioned on the left (L) and right (R) sides of the

https://doi.org/10.5194/egusphere-2026-59
Preprint. Discussion started: 28 January 2026

beam. These arrays measure chords across the particle's diffraction pattern, providing optical scattering information, serving as proxies for morphology. The arrays are offset from the beam centerline by a distance set for the instrument's target particle size range. Consequently, the morphology metrics derived from diffraction are inherently size-dependent because diffraction pattern scales vary with particle size, whereas the array spacing is fixed. Fluorescence emitted after excitation is collected by a hemispheric mirror, dispersed using a diffraction grating, and measured in eight acceptance intervals (bands, channels) with roughly equidistant central wavelengths spanning approximately 315-640 nm (Fig. S3). Fluorescence intensity is not measured in physical units; we report absolute fluorescence as a detector signal in arbitrary units (au). Fluorescence signals in individual channels may saturate if intensities exceed the detector's upper sensitivity limit. The maximum particle measurement rate is also limited by the xenon lamp's recharge time, yielding an upper rate of about 100 particles s^{-1}.

2.2 Data treatment

The MBS periodically measures the background fluorescence, i.e. without sample flow, once when beginning the measurement and then typically after 30,000 samples. This provides an estimate of the instrument's baseline, which is subtracted from each particle's measured spectrum. Fluorescence intensity can be expressed in terms of standard deviations (σ) above the mean background. Because the MBS's sampling efficiency drops below 50% for sizes $<$0.8 µm (Ruske et al., 2017), we exclude all particles smaller than this from our analysis. Particle morphology parameters are calculated by the MBS software from the two CMOS array scattering signals. These parameters distill characteristics of particle scattering properties into statistical and shape descriptors. For each array, the software calculates the mean and variance of signal intensity, as well as the skew and kurtosis (treating each detected curve as a normal distribution). It also locates peaks using a user-defined local peak-trough threshold and derives peak width (width at half maximum of the strongest peak), peak-to-mean ratio (PTMR; also based on the strongest peak), and peak count for each array. Mirror symmetry, defined as the similarity between the bottom and top halves of the signal, is calculated for each array and given as a percentage. Because particles align with the flow and have arbitrary rotational orientations in the detection stage, we report array-specific parameters using an arbitrary array of choice (right; R) for visualization. Two additional asymmetry parameters are provided: left-right (L-R) pixel-wise asymmetry, and pixel-wise asymmetry with one array inverted, both calculated as a percentage.

Freitas et al. (2022) developed a heuristic decision tree (DT)-based classification of particles measured by the MBS based on fluorescence, which was later applied and validated in subsequent studies (Freitas et al., 2023a; Zinke et al., 2024; Freitas et al., 2024; Kojoj et al., 2024). In this classification scheme (Fig. 2 in Freitas et al. 2022), particles are classified as fluorescent (3-9σ fluorescence in any channel), highly fluorescent particles (HFPs; $>9\sigma$ signal in any channel), and fluorescent PBAPs (fPBAPs), defined as HFPs with a fluorescence maximum in the second (B) channel. It is well documented that PBAPs, especially bacteria, commonly show pronounced fluorescence around 350-400 nm due to fluorophores such as tryptophan (Pöhlker et al., 2012). This feature underpins the MBS's design and is widely used in UV-LIF-based PBAP detection (e.g. Crawford et al. 2015; Tang et al. 2022; Gao et al. 2024). In this study, we used this DT-based method as a benchmark for PBAP identification. As an additional metric of the shapes of fluorescence spectra, we calculate a fluorescence ratio defined as the sum of channels A and B divided by the sum of channels C-H, with higher values indicating a stronger peak in the earlier channels.

https://doi.org/10.5194/egusphere-2026-59
Preprint. Discussion started: 28 January 2026

2.3 Samples and laboratory characterization experiments

The samples characterized with the MBS in this study are selected to represent aerosols relevant to the Northern Hemisphere, including boreal/tree pollen, marine bacteria, dust, and synthetic contaminants (Table 1). Cellulose, a major component of plant cell walls, was chosen as an analog to plant matter debris and as a constituent of pollen (e.g. Winiwarter et al. 2009; Yttri et al. 2011; Bozzetti et al. 2016). We used pure, synthesized crystalline cellulose (Sigma Aldrich, cat. no. 435236) ground into particles.

Pollen were sourced from various locations in the Czech Republic by Pharmallerga CZ s.r.o. (Lišov, Czech Republic). The species of trees from which pollen was sourced for this study were ash (*Fraxinus excelsior*), black alder (*Alnus glutinosa*), birch (*Betula pendula*), hazel (*Corylus avellana*), juniper (*Juniperus communis*), Scotch pine (*Pinus sylvestris*), and willow (*Salix caprea*). Pharmallerga assessed pollen quality by microscopy and with acetic blue staining; pollen processing and size ranges they reported are listed in Table S1. Pollen were collected by hand, with the exception of juniper, which was collected with vacuum. All samples were processed dry (sifting and drying), with the exception of willow, which was defatted with acetone. To investigate whether aerosolization method affected MBS-observed properties, we used both dry and wet nebulization.

Bacterial samples were mixed cultures of cyanobacteria from Baltic seawater. We selected three cultures with distinct natural pigment profiles (phycobiliproteins and carotenoids) to capture diversity, but we did not identify individual species. These pigments – phycobiliproteins (phycoerythrin, phycocyanin, and allophycocyanin) and other compounds (e.g. carotenoids) – absorb in different spectra of light and differ from chlorophyll A absorption (Gantt and Cunningham Jr, 2001), allowing them to be differentiated from algae.

Ground polyethylene (PE) was chosen as a representative microplastic. Because environmental microplastics undergo weathering processes that may alter their optical and fluorescence properties, we measured freshly ground PE particles, with one subsample exposed to UV light to simulate photolytic aging.

Natural dust samples from four sources, Dyngjusandur and Myrdalssandur in Iceland, Svalbard, and Sakurajima in Japan, were included as potential high-latitude dust sources relevant to the Arctic. Dyngjusandur and Myrdalssandur samples contain primarily volcanic silt and sand (Arnalds et al., 2016), whereas the Sakurajima sample is primarily volcanic ash. The Svalbard sample, previously characterized for its ice nucleation activity in Tobo et al. (2019) (sample BR1607b), originates from glacial outwash sediment. In addition, kaolinite clay was selected as a sample of mineral dust reference expected to contain minimal organic matter.

For dry, solid materials, 5 ml of the sample was placed in a centrifuge tube mounted on a speaker (Fig. S4b) and vibrated at a frequency selected using a function generator. The optimal frequency depended on the sample type and nebulization efficiency, but stable, high particle concentrations were typically achieved at 15-30 Hz. A commercial nebulizer (Topas GmbH, Germany, model ATM228) with a fixed nebulization pressure of 100 hPa (gauge) was used for wet and liquid samples, including pollen solutions. For wet nebulization using the TOPAS nebulizer, the sample air stream was dried using a Nafion dryer, while the sample air from the dry (speaker) nebulization was not actively dried (see Fig. S4). The sample air relative humidity was monitored using an inline RH/temperature sensor (Hytelog USB, B+B sensors, Germany) immediately upstream of the MBS

https://doi.org/10.5194/egusphere-2026-59
Preprint. Discussion started: 28 January 2026

to ensure particles were measured dry. Each sample was nebulized and measured for at least 10 minutes. Background tests using empty containers (shaken empty centrifuge tubes for dry samples, nebulized pure Milli-Q water for wet) showed negligible background concentrations, far below those seen in the characterization experiments ($O(10^0)$ L^{-1}). Samples were measured in sequence from those least to most likely to adhere to the instrument and plumbing to minimize carryover between experiments.

2.4 External data

To compare our characterization of specific aerosol types to previous work, we include laboratory data from Ruske et al. (2017), Crawford et al. (2020), and Beck et al. (2024), as well as data from known pollution events in Karlsson et al. (2022). The pollution events were observed during an Arctic Ocean research cruise, when the ship's plume was sampled directly by the inlet housing the MBS. Because the ship operated in very remote locations (>80° N) and particle concentrations during the pollution events exceeded background concentrations of other fluorescent particles (e.g., PBAPs) by several orders of magnitude, we consider these observations representative of fossil fuel combustion sources, despite being measured in ambient air. The sea spray aerosol (SSA) measured by Beck et al. (2024) were generated with a plunging-jet sea spray simulation chamber of the type described by Salter et al. (2014) and Salter et al. (2015). We include data from our characterization experiments and these external sources in our ML training and classification algorithm (see Section 2.5). This extends the classes of particles to include fungal spores (Crawford et al., 2020) and SSA (Beck et al., 2024), and increases diversity in bacteria, pollen, and dust samples (Ruske et al., 2017; Crawford et al., 2020; Beck et al., 2024). Table 1 lists source type, used nebulization methods, and citations for all data considered in our study, including our own characterization experiments.

2.5 Machine learning and classification algorithm

Information from the MBS can be used to train particle identification algorithms on laboratory characterization data; such approaches using ML have previously been applied to measurements made with the MBS (Ruske et al., 2017) and other UV-LIF spectrometers (Ruske et al., 2018). Here, we develop a new and improved classification algorithm for MBS data with three objectives, in order of priority:

1. flag fluorescent particles that are likely interferents, so they can be excluded from PBAP concentration estimates;
2. classify fluorescent particles into broad bioaerosol subgroups, and;
3. classify non-fluorescent particles as dust- or SSA-like particles.

The methods used for each component model are described below, with their implications discussed in the results (Section 3.3). Supplementary Table S2 summarizes the MBS data input variables and their roles in the classification algorithm.

We treated tasks 1 and 2 as binary classification tasks and used logistic regression modeling (LRM; El Morr et al. 2022) for both. LRMs fit logistic functions to training data to estimate the probability that a new observation belongs to class 0 or 1, and can accomodate many input variables. This approach is well suited to task 1, flagging observations as interferents or non-interferents, and to the dust vs. non-dust decision in task 3. The model output is a probability estimate between 0 and 1, obtained by averaging logistic function outputs across input features. Positive identification can be determined by rounding this

https://doi.org/10.5194/egusphere-2026-59
Preprint. Discussion started: 28 January 2026

Class category	Sample	Source	Nebulization
Cellulose	Pure shredded cellulose	This study	Dry
Dust	Volcanic sand from Myrdalssandur, Iceland	This study	Dry
	Volcanic sand from Dyngjusandur, Iceland	This study	Dry
	Volcanic ash from Sakurajima, Japan	This study	Dry
	Glacial outwash sediment from Svalbard, Norway	This study	Dry
	Kaolinite clay dust	This study	Dry
Microplastics	Shredded PE	This study	Dry
	Shredded PE, aged with UV light	This study	Dry
	Polystyrene latex (PSL) spheres	Beck et al. (2024)	Wet
Pollen	Black alder (*Alnus glutinosa*) pollen	This study	Dry and wet
	Ash (*Fraxinus excelsior*)	This study	Dry and wet
	Birch (*Betula pendula*)	This study	Dry and wet
	Hazel (*Corylus avellana*)	This study	Dry and wet
	Juniper (*Juniperus communis*)	This study	Dry and wet
	Scotch pine (*Pinus sylvestris*)	This study	Dry and wet
	Willow (*Salix caprea*)	This study	Dry and wet
	Aspen (*Populus tremula*)	Ruske et al. (2017)	Dry
	Paper mulberry (*Broussonetia papyrifera*)	Ruske et al. (2017)	Dry
	Poplar (*Populus nigra*)	Ruske et al. (2017)	Dry
	Ryegrass (*Lolium perenne*)	Ruske et al. (2017)	Dry
Bacteria	Baltic seawater sample culture (60BSN)	This study	Wet
	Baltic seawater sample culture (B10, B6)	This study	Wet
	Baltic seawater sample culture (B9, B6)	This study	Wet
	Escherichia coli cultured in L-broth	Ruske et al. (2017)	Wet
	Picocyanobacteria isolate in filtered seawater	Beck et al. (2024)	Wet
Fungal spores	*Alternaria alternaria* spores	Crawford et al. (2020)	Dry
	Cladosporium herbarium spores	Crawford et al. (2020)	Dry
Sea spray aerosol	Filtered Arctic seawater	Beck et al. (2024)	Wet (sea spray tank)
	Artificial sea salt	Beck et al. (2024)	Wet (sea spray tank)
Combustion	Ship smokestack plume	Karlsson et al. (2022)	Ambient

Table 1. Overview of the analyzed samples, their citations, and nebulization methods used in their source experiments.

185 probability or by choosing a threshold, which can adjust identification confidence. Our LRMS were trained using least squares error (L2) loss functions and the limited-memory Broyden-Fletcher-Goldfarb-Shanno (LBFGS) solver (Nocedal, 2006).

https://doi.org/10.5194/egusphere-2026-59
Preprint. Discussion started: 28 January 2026

Dimensionality reduction is useful for quantifying and presenting differences between observations with a high number of features (Jia et al., 2022), such as the many fluorescence and morphology metrics measured by the MBS. Incorporating morphology metrics into particle classification can help prevent overly strong influence by fluorescence information, which may not be enough to distinguish particle types. Dimensionality reduction can be used to rapidly map similarities with known particles and as a pre-processing step for other ML methods, or as its own classification method (Crawford et al., 2020, 2023) in certain cases. For task 2, we used uniform manifold approximation and projection (UMAP), a technique for approximating a topological manifold on which data with any number of dimensions are located and quantifying their relative proximities in a lower dimensional space. UMAP approximators are created by iteratively considering n neighbors in the dataset and estimating proximities between members, projecting the graph in e.g. two-dimensional space, and ensuring that connections between individual points in the original data are preserved (Healy and McInnes, 2024). Our UMAP approximators were made using the UMAP-learn Python library; details about the package's methods and underlying theory are described in McInnes et al. (2020). For training, we used 100 neighbors, set a minimum separation between transformed points of 0.5, and provided training class labels for clustering. The approximator's outputs are the transformed data positions in two arbitrary dimensions, here defined as UMAP_1 and UMAP_2, similar to other non-metric multidimensional scaling methods (e.g. Clarke 1993).

After UMAP transformation, we used k-nearest neighbors (kNN) to classify data according to their positions in the transformed space relative to the positions of particles of known types from source characterization data. In kNN, observations are compared to the k closest neighbors in the training data and classified by votes defined as the number of neighbors belonging to each class. The kNN outputs a class identification corresponding to the class with the most votes and the percentage of votes among the k neighbors cast for each class. Because kNN classifiers generally struggle with high-dimensional data, the use of UMAP both simplifies class labeling (compared to other multiclass methods such as random forest) and provides an additional clustering step for more robust identification.

2.6 Algorithm validation and domain adaptation

To assess our classification algorithm, we applied it to MBS observations from Zeppelin Observatory, Svalbard made over 2020 during the Ny-Ålesund Aerosol Cloud Experiment (NASCENT) campaign (Pasquier et al., 2022). This reproduces the analysis of Freitas et al. (2023a), who applied and further validated the fluorescence-only DT-based approach that has since proven succesful in other studies made with the MBS (Freitas et al., 2024; Zinke et al., 2024; Kojoj et al., 2024). Repeating this published analysis with our new classification algorithm allows a direct assessment of its strengths and weaknesses. Additional data for validation were obtained from 24 hour to weekly resolved filter sampling (Platt et al., 2022), except for equivalent black carbon (eBC), which was obtained with the Multiangle Aerosol Absorption Photometer (MAAP) at minutely resolution averaged to daily values (Freitas et al., 2023a). Sampling frequencies and references for the species (tracers) used for the validation here and in Freitas et al. (2023a) are summarized in Table S3. Both classification algorithms were applied to MBS data collocated with the tracer sampling windows. Particle class concentrations were calculated as the number of observed particles assigned to each class divided by the MBS sample air volume during that period. Sample volume was determined from the sampling duration and the and the constant sample flow rate of 0.33 L min^{-1} reported in Freitas et al. (2023a).

https://doi.org/10.5194/egusphere-2026-59
Preprint. Discussion started: 28 January 2026

We use chemical tracers for dust (silicon, iron, potassium) (Lu et al., 2019; Bai et al., 2021; Hird et al., 2024), PBAP (fructose, glucose, arabitol, and mannitol) (Bauer et al., 2008; Winiwarter et al., 2009), SSA (sodium, chloride, magnesium, calcium) (Crawford et al., 2019; Karle et al., 2024), anthropogenic aerosol (eBC), and biomass burning (eBC, levoglucosan) (Vincenti et al., 2022). Fructose and glucose are monosaccharides used as PBAP tracers (Jia and Fraser, 2011). Glucose is ubiquitous across organisms, whereas fructose is a photosynthetic product rapidly metabolized by non-plant organisms and is thus more characteristic of pollen and plant matter (Pacini et al., 2006; Medeiros et al., 2006; Jia et al., 2010; Rathnayake et al., 2017; Mampage et al., 2022). Arabitol and mannitol are sugar alcohols that serve as energy reserves and, owing to their abundance in fungi, are considered as tracers for fungal spores (Bauer et al., 2008), and have been used to verify UV-LIF-based fungal spore detection (Gosselin et al., 2016). Levoglucosan forms from the pyrolysis of cellulose and is an established tracer for biomass burning (BB) (Simoneit, 1999; Yttri et al., 2015; Xu et al., 2018; Yttri et al., 2024). eBC is emitted by both fossil fuel and biomass combustion and is thus used to trace the influence of all combustion aerosols (Andreae and Gelencsér, 2006).

Having simultaneous knowledge about particle composition from detailed tracer data also affords the possibility of directly implementing lessons from the validation assessment in tuning the classification algorithm, a process known as transfer learning (Venkateswara and Panchanathan, 2020). Domain adaptation is a ML technique for transfer learning wherein a model trained in one domain (here, in laboratory settings) is adapted for use in another (field observations), which helps overcome challenges introduced by differences between the domains (e.g. differences in particle properties between naturally and laboratory-generated aerosol). We implemented domain adaptation in our classification algorithm based on the results of the validation by using tracer concentrations to construct probability estimates of observing targeted particle types, which were used to further train the model in a controlled manner. The details of the domain adaptation implementation are further explained alongside our assessment of the initial classification algorithm in Section 3.4 and in the SI.

3 Results

3.1 Laboratory characterization of fluorescent particles

Emission spectra and size distributions for dry and wet pollen samples are shown in Fig. 1. The particles we detected are far smaller than the whole pollen grain sizes reported by the supplier (Table S1); our results therefore represent sub-pollen particles (SPPs) produced by the rupture or fragmentation of whole pollen grains. Moisture (Suphioglu et al., 1992; Stone et al., 2021; Matthews et al., 2023) and impaction (Visez et al., 2015) are known to induce rupture and SPP emission in laboratory experiments and in ambient air, providing a secondary source of PBAPs with a greater transport range and residence time than whole pollen. SPPs may therefore impact key atmospheric processes (Wozniak et al., 2018; Hughes et al., 2020; Prank et al., 2025). Although their ambient detection remains difficult, observational evidence of strong variability in SPP emission and concentrations under humid conditions has been found using UV-LIF (Hughes et al., 2020; Zhang et al., 2025). While our data should aid SPP identification in field observations, it is important to note that intact pollen grains lie outside the MBS's detection size range and cannot be measured with this instrument. Additionally, rupture and/or fragmentation may have been promoted during transport and storage.

https://doi.org/10.5194/egusphere-2026-59
Preprint. Discussion started: 28 January 2026

Most dry pollen samples peak in the *C* channel (∼414 nm), with ash, juniper, and pine having slightly broader spectra. Wet nebulization consistently broadens spectra occurs of all pollen tested and shifts maxima to channel *D* (∼461 nm). Dry pollen fluourescence is dominated by fluorophores on the grain exterior, composed mainly of sporopollenin (Zimmermann, 2010), whereas SPPs can include interior fluorophores, such as phenols, carotenoids, azulene, and anthocyanin, all with different emission characteristics (Fennelly et al., 2018). Wet nebulization produced more numerous, smaller particles than dry nebulization, indicating a different SPP emission mode, likely including soluble material re-formed as residue after drying. Such particles would tend to show more droplet-like scattering signatures (Section 3.3). Thus, the aerosolization method clearly affects both fluorescence and morphology, with implications for ambient detection. The especially strong wet-dry contrast in willow pollen fluorescence (Fig. 1g and 1n) may be due to acetone de-fatting (Table S1), as removing surface lipids likely increase water uptake and solubility, promoting rupture and altering fluorescence.

Figures 2a-c show that fluorescence spectra recorded for bacteria are dominated by a *B* channel peak, consistent with Pöhlker et al. (2012) and Huffman et al. (2020), and the decision tree criterion of Freitas et al. (2022). This feature is unique among our samples and provides a robust marker for fPBAP identification. In contrast, PE, both fresh and UV-aged, and cellulose (Fig. 2d-f) constitute potential interferents. PE spectra closely resemble those of dry pollen with *C* channel maxima, and cellulose shows similar pollen-like fluorescence. While atmospheric coarse-mode microplastic concentrations are unlikely to be high enough to strongly bias PBAP detection, these results show that synthetics can mimic the fluorescence properties of fPBAPs. Cellulose-fPBAP similarity (Fig. 2f and 2l), however, is relevant for the atmosphere because cellulose-containing plant debris may be abundant (Hiranuma et al., 2015, 2019). Being PBAPs themselves, they may be less of a complicating factor in UV-LIF detection, although this depends on classification precision requirements. Our pure cellulose spectra agree with published measurements of cellulose (Kulpinski et al., 2012) and the *C* channel peak may contribute to pollen signals because the pollen intine is cellulose-rich and can be exposed during fragmentation (Hess, 1993; Fang et al., 2008). Among all fluorescent samples measured here (Figs. 1 and 2), fluorescence intensity increases with size, as expected from the larger amount of emitting material, implying that fluorescence contrast among smaller particles are inherently muted compared to larger particles.

3.2 Fluorescence and morphology characteristics across all sources

Here we present the results of all source characterization experiments and MBS observations used in this study (Table 1), processed as described in Section 2.2. Figure 3 summarizes fluorescence emission spectra for all fluorescent materials, and Fig. 4 presents class contributions and select morphology parameters. Pollen spectra from our experiments (Fig. 3b-o) and those of Ruske et al. (2017) (Fig. 3p-s) show broader spectra and higher intensities than bacteria (Fig. 3t-x). Despite many highly fluorescent particles (Fig. 3a), only a small fraction ($O(10^{-2}\text{-}10^{-1})\%$) from our pollen samples is classified as fPBAP by the Freitas et al. (2022) DT. This indicates that a substantial share of pollen-derived particles would be missed by fluorescence-only schemes, but the variable peak channels (Fig. 1 and 3b-s) make it difficult to define a robust single-channel classification criterion.

https://doi.org/10.5194/egusphere-2026-59
Preprint. Discussion started: 28 January 2026

Bacteria samples from Ruske et al. (2017) and Beck et al. (2024) exhibit the same *B* channel peak and similar intensities as our bacteria samples, reinforcing the robustness of the DT-based fPBAP criterion of Freitas et al. (2022). Fungal spores fluoresce more strongly than bacteria and often peak in both channels *B* and *C*, meaning some fungal spores will be missed by the DT method. We find that polystyrene latex spheres (PSLs) (Fig. 3cc) closely resemble bacterial *B* channel peaks, and all highly fluorescent PSLs meet the DT definition of fPBAP (Fig. 4a), demonstrating that synthetic particles can mimic bioaerosols in UV-LIF measurements. We also find that the diesel combustion particles from Karlsson et al. (2022) exhibit broad, intense fluorescence (Fig. 3dd) and that about 10% of them meet the DT-based fPBAP criterion (Fig. 4a), consistent with complications noted in Freitas et al. (2023a, 2024). Because combustion particles from fossil fuel and BB are abundant in the atmosphere, their fluorescence similarity to bioaerosols is a primary concern for PBAP quantification. Using instruments with multiple excitation wavelengths, such as the WIBS (Markey et al., 2024), can add discriminating power; despite higher spectral resolution in fluorescence emission detection, the MBS is limited in this regard, motivating a combined fluorescence-morphology classification approach.

Beyond fluorescence, the MBS provides extensive optical scattering-based morphology information (Fig. 4b-f), which offers additional leverage against synthetic and combustion interferents. For clarity, we show morphology parameter distributions for <3 µm and ≥ 3 µm particles. Importantly, interpretation must account for different emission mechanisms for various bioaerosols. Bacteria and many fungal spores fall within the MBS's size range and may be detected intact, whereas pollen rupture and plant debris emission generate irregular fragments with highly variable shapes. Fungal spores can also fragment under prolonged exposure to high humidity (China et al., 2016; Subba et al., 2021). Accordingly, pollen, and to some extent fungal spores, tend to have more irregular morphologies, whereas bacteria and intact spores exhibit more regular scattering signatures (Fig. 4c-f). Combustion particles, aside from their high peak counts, also exhibit scattering signatures indicative of irregular morphologies. This may help to distinguish them from bacteria and fungal spores but not necessarily from pollen-derived particles. Consistent with the discussion in Section 3.1, wet nebulized pollen show more spherical morphologies, indicating that many particles are dried residues of dissolved constituents rather than physical fragments.

Figure 4c-f and Fig. S5 compare dust, nascent SSA (Beck et al., 2024), and PSLs (Beck et al., 2024) (a spherical, opaque reference particle). Dust and SSA particles differ clearly in mean signal (Fig. 4d), peak count (Fig. 4f), variance (Fig. S5e), and peak width (Fig. S5i), even at smaller sizes. L-R asymmetry is broader and more extreme for dust, although overlap remains (Fig. 4c). Surface roughness is reflected in signal mean, PTMR, and peak count (Fig. 4d-f, respectively), as well as in variance, kurtosis, and peak width (Fig. S5e, g, and i, respectively). Rough surfaces smear diffraction patterns, raising scattering signal mean and variance, reducing the number of distinct peaks, and increasing peak width and PTMR. Our dust samples show lower peak counts and higher signal mean and variance, PTMR, and peak widths than SSA and PSLs, indicating rougher, more irregular surfaces. Dust also shows higher and broader skewness distributions (Fig. S5f), consistent with irregular shapes. Strong smearing by diffraction on rough surfaces can increase mirror symmetry, which may explain the relatively high mirror values seen in dust (Fig. S5c).

In summary, dust exhibits high surface roughness and shape irregularity, whereas SSA shows sharper diffraction features and lower asymmetry. These features are consistent among all dust samples measured here, with small differences in size dis-

https://doi.org/10.5194/egusphere-2026-59
Preprint. Discussion started: 28 January 2026

tributions (Fig. 4b). Dust sample fluorescence varies (Fig. 4a), with the fuller's earth sample (Ruske et al., 2017) standing out, possibly indicating the presence of fluorophores such as humic substances (Pöhlker et al., 2012). Some of the consistency in measured dust features may derive from the generation method, which can bias certain particle sizes and alter their properties (Gill et al., 2006). SSA morphology is known to vary with size (Kaluarachchi et al., 2022), source conditions such as productivity and organic content (Lee et al., 2020), wind speed at emission Madawala et al. (2024), and atmospheric processing (Kaluarachchi et al., 2022). However, the SSA samples considered here are freshly generated, representing nascent particles; how aging affects MBS scattering and fluorescence signatures thus remains an open question.

3.3 Particle classification by machine learning

Using the source characterization data presented in Section 3.2, we build classification models as a basis for an algorithm for (1) distinguishing fPBAPs from interferents among fluorescent particles, (2) attributing them to broad fPBAP classes, and (3) distinguishing between non-fluorescent dust- and SSA-like coarse-mode particles. For (1), we consider only combustion particles as interferents due to limited synthetic polymer sample diversity in our training data and because they are likely far more abundant than microplastic particles in the atmosphere. This simplifies the task to binary classification (pollution or not). For (2), we divide fPBAPs into three classes: pollen, bacteria, and fungal spores; cellulose is not represented because real plant debris was not included in the source characterization data. Binary classification was also used for (3) to estimate dust- or SSA-likeness among non-fluorescent particles. These components were implemented in the classification algorithm presented in Fig. 5 (given in written form in Table S4), which also presents the DT method of Freitas et al. (2022) for comparison.

In our algorithm, particles are first filtered according to fluorescence; highly fluorescent $\geq 9\sigma$ particles are passed to the pollution and fPBAP identification branch, while the remaining particles $\geq 2.5\,\mu m$ are passed to the dust/SSA branch. Particles in the fluorescent branch are first assigned a pollution-likelihood (p_{pol}) by the pollution model, and are then fed to the UMAP approximator. UMAP outputs are passed to the kNN classifier, which provides class likelihoods for four target classes (pollution, pollen, bacteria, and fungal spores). A fluorescent particle's p_{pol} must not surpass a confidence threshold (α_{pol}) for it to be classified as a fPBAP. Thus, the algorithm uses a two-step identification process for fPBAPs where a fluorescent particle must be both not flagged as an interferent by the pollution model and positively identified as one of the fPBAP classes by the multiclass model. The multiclass model's outputs also allows a further confidence threshold for fPBAP identification to be chosen based on the kNN's probability estimates. Particles $\geq 2.5\,\mu m$ in the non-fluorescent branch are assigned a dust-likelihood (p_{dust}) by the dust model. This may be used for identification based on a confidence threshold (α_{dust}) or as a metric itself ("dust-likeness"). In our assessment, we used the most likely class (the rounded probability for LRMs and the class of highest probability for the kNN) for identification.

As inputs for the pollution LRM and UMAP approximator, we used 34 features, including: normalized fluorescence spectra, fluorescence ratio, total fluorescence, size, L-R asymmetries (top-to-bottom and inverse), and scattering parameters for L and R arrays (nine each). The UMAP approximator was fitted only on highly fluorescent combustion, pollen, bacteria, and fungal spore particle data, and excluded cellulose and microplastics; the limited diversity represented in our data for these latter two classes would likely affect the generalizability of a ML-based approach. However, UMAP transformations were calculated

https://doi.org/10.5194/egusphere-2026-59
Preprint. Discussion started: 28 January 2026

for microplastics and cellulose to quantify their similarities with the other classes. After transformation, fluorescent particles can be classified according to their proximity in UMAP phase space to clusters seen in the training data. We trained a kNN classifier on UMAP-projected source characterization data, which uses a brute force global search of training data positions in UMAP space to select the 100 closest neighbors ($k = 100$) according to Euclidean distance. The probability that the unknown particle belongs to each class is the fraction of neighbors belonging to them, weighted inversely by distance.

Table 2 presents confusion matrices for each ML model included in the algorithm. The pollution LRM performs well on testing data, identifying combustion particles with 92% precision. Figure 6a shows UMAP projections for fluorescent particles using only pollen, bacteria, fungal spores, and combustion particles for training, illustrating clear separation between combustion particles and all fPBAP classes; the clearer the separation between clusters, the more certainty can be obtained in discriminating between them. The positions of particles in classes unknown to the UMAP (microplastics and cellulose) are distributed among the three fPBAP classes, indicating similarities shared with each of them. Few microplastic particles appear near the combustion particle cluster, and cellulose particles are mostly positioned near the pollen cluster. These relations between particle clusters in UMAP space reflect their similarities discussed in Section 3.2, indicating that the UMAP approximator effectively separates clusters of broad fluorescent particle classes and captures similarities between them.

Figure 6b shows UMAP transformations of the testing data and illustrates that the approximator also produced the general distributions and locations of class clusters seen in Fig. 6b with unknown particles. Lower certainty can be expected where significant overlap exists between clusters, manifested in lower kNN prediction probabilities at midpoints between clusters. Most fPBAP incorrectly classified as combustion particles were pollen and fungal spores, and combustion particles that were wrongly classified as fPBAP are exclusively pollen; the UMAP-kNN classifier model misclassified combustion particles as pollen ∼11% of the time (Table 2). This reflects similarities between combustion and pollen particles discussed in Section 3.2 (e.g., their broad fluorescence curves). Among fPBAP classes, the UMAP-kNN classifier was weakest at identifying bacteria, and significant confusion between certain fungal spores and bacteria were seen; ∼16% of bacteria particles were misclassified as fungal spores. This may be expected given their similarities in spectral maxima, and because the UMAP-kNN method incorporates morphology information that also determines classification.

For the dust model, we trained a LRM on 22 morphology parameters (top-to-bottom and inverse L-R asymmetries and the nine chord shape parameters for each side; see Table S2). We disregarded particle size in the dust LRM to reduce the influence of biases introduced to the training data by laboratory aerosolization methods via their size distributions, and focused the method of distinction on distributions of optical scattering properties. Following the discussion around Fig. 4, we trained only on dust and SSA particles ≥2.5 µm to ensure more distinct separation between their scattering signatures. Equal samples of 6,000 particles each were randomly drawn from this size range. The LRM converged quickly (23 iterations) and testing resulted in 99% precision for both classes (Table 2), indicating that the distributions of optical morphology parameters are distinct enough to accurately distinguish them. Training the same LRM using all particles ≥0.8 µm resulted in a slight decrease in the model's overall precision (95%). Despite this, we argue that training particles in a size range where the instrument better resolves optical scattering signatures produces a more physically sound model and elected to use the LRM trained only on ≥2.5 µm particles in our classification algorithm.

https://doi.org/10.5194/egusphere-2026-59
Preprint. Discussion started: 28 January 2026

Actual	**Predicted**			
Pollution model				
	False	True	–	–
False	**0.987 (1890)**	0.013 (25)	–	–
True	0.079 (25)	**0.921 (293)**	–	–
Fluorescent particle classifier				
	Combustion	Pollen	Bacteria	Fungal spores
Combustion	**0.887 (282)**	0.113 (36)	0.0 (0)	0.0 (0)
Pollen	0.021 (17)	**0.843 (685)**	0.001 (1)	0.135 (110)
Bacteria	0.0 (0)	0.024 (3)	**0.821 (101)**	0.155 (19)
Fungal spores	0.010 (8)	0.114 (96)	0.001 (1)	**0.876 (741)**
Dust model				
	Dust	SSA	–	–
Dust	**0.992 (1190)**	0.008 (10)	–	–
SSA	0.014 (17)	**0.986 (1183)**	–	–

Table 2. Confusion matrices for the pollution, bioaerosol classification, and dust model components of our classification algorithm. Pollution and dust models are based on logistic regression, and the multiclass classification is based on uniform manifold approximation and projection (UMAP) and k-nearest neighbors (kNN) models. The fraction of testing data predicted as each class is given in columns along with the number of testing data points in parentheses; fractions therefore sum to one across rows. The recall for a given class is identified in bold.

3.4 Classifier domain adaptation and validation

Figure 7 presents the results of our classification algorithm applied to MBS observations made by Freitas et al. (2023a) at Zeppelin Observatory during 2020, again using simple majority classification thresholds for pollution and dust ($\alpha_{\text{pol}}, \alpha_{\text{dust}} = 0.5$). The algorithm, trained only on source characterization data, struggled to recognize the types of combustion particles seen at Zeppelin Observatory, as evidenced by the high correlation between fPBAP concentrations and levoglucosan and eBC (Fig. S7b). The fact that fPBAP concentrations correlated more strongly with levoglucosan than with eBC may suggest an influence by specific combustion particle types, i.e., BB- rather than fossil fuel-derived. Biological tracer and DT-based (Freitas et al., 2023a) fPBAP concentrations indicate a clear seasonal cycle of biological aerosol influence, which our algorithm initially failed to capture (Fig. 7b). This resulted in likely overestimated fPBAP concentrations, especially evident between January-April when eBC concentrations were high.

To address this, we apply domain adaptation to tune the pollution LRM to HFPs observed at Zeppelin Observatory using tracer-based soft labels describing the degree of pollution vs. biological dominance. This is accomplished by choosing a number of sample periods with sufficient tracer data and labeling HFPs observed during these periods as either pollution or not based

https://doi.org/10.5194/egusphere-2026-59
Preprint. Discussion started: 28 January 2026

on the soft label, and further training the LRM on these data (the tuning block) with lower weights than those of the initial training data to limit its influence on model fit; details of this step are explained the SI. The pollution influence metric was calculated using normalized eBC and arabitol concentrations, and the combined weighting of the tuning block on the LRM's fitting was set to 20% of the training data's. Individual weights were calculated for tuning data based on this scaling and our confidence in the soft labels, determined by the pollution influence metric.

The tuned fluorescent particle classifier reproduces the DT-based fPBAP concentration time series (Freitas et al., 2023a), with few ($\sim 10^{-3}$-10^{-1} L^{-1}) fPBAP during winter and early spring, a peak in July, and a subsequent decrease during winter onset (Fig. 7a-b). The high proportion of HFPs labeled as interferents between January and April (Fig. 7a), along with significant correlations between the pollution class and lead eBC, and levoglucosan (Fig. 7e), shows that the classification algorithm robustly reduces the influence of combustion particles. In August, when biological tracer concentrations were highest, our algorithm detected fPBAP concentrations nearly two orders of magnitude higher than the DT method did. This is expected because the DT-based fPBAP criterion is validated for one type of fPBAP, while our classification algorithm targets multiple fPBAP types with diverse fluorescence properties. Using scanning electron microscopy, Tobo et al. (2024) determined that most carbonaceous coarse-mode particles sampled at Zeppelin Observatory in July 2020 were likely PBAPs (such as microorganisms and plant debris), while none were detected in March 2020. The low (high) proportion of HFPs classified as fPBAPs during March (July) reflects a similar seasonal fPBAP cycle as that described in Freitas et al. (2023a). Both our algorithm's and DT-based fPBAP concentrations correlate significantly with BB tracers (Fig. 7e), in agreement with Freitas et al. (2023a). Although levoglucosan is formed only through pyrolysis, incomplete biomass combustion can release monosaccharides (e.g., glucose, fructose) when wood carbohydrates (e.g., cellulose) are broken down (Medeiros et al., 2006; Zangrando et al., 2016; Ren et al., 2020; Vincenti et al., 2022). This has implications for the interpretation of fructose and glucose as PBAP tracers, as illustrated by their correlations with levoglucosan (Fig. S8).

Pollen contributes the largest class share to fPBAP by our algorithm throughout the year but more consistently in summer, followed by fungal spores and bacteria (Fig. 7c). A portion of the fPBAP class may be combustion particles falsely identified as pollen due to their similarities described in Sections 3.2 and 3.3. Another portion may be fungal spores misclassified as pollen, as evidenced by their similar behaviors in correlations with fungal tracers. Bacteria makes up a small proportion ($\sim$0.1-1%) of fPBAP identified by our classifier. Unfortunately, contributions by specific fPBAP classes are difficult to validate with tracer data available at Zeppelin Observatory for this time. Although arabitol and mannitol are considered fungal tracers, they can be found to lesser degrees in pollen and bacteria (Lau et al., 2006; Di Filippo et al., 2013). PBAP analyzed by Freitas et al. (2023a) and Tobo et al. (2024) with electron microscopy could not be precisely distinguished, although visual comparison suggested that they were likely fungal spores and bacteria. Tobo et al. (2024) also found irregular carbonaceous particles resembling plant debris, a globally abundant PBAP (Sánchez-Ochoa et al., 2007; Winiwarter et al., 2009), or possibly pollen fragments. Considering the similarities between pollen, fungal spores, and pure cellulose seen in Sections 3.2 and 3.3, plant debris not flagged as combustion particles would likely be classified as pollen- or fungal spore-like by our classifier due to their broad fluorescence spectra (as in Fig. 6a). Furthermore, plant debris can be emitted by BB (Holden et al., 2011), with the degree of similarity to smoke particles depending on the degree of influence by combustion. This may be reflected in the correlations

https://doi.org/10.5194/egusphere-2026-59
Preprint. Discussion started: 28 January 2026

between fPBAP detected by our algorithm and BB tracers (Fig. 7e), and between cellulose and levoglucosan (Fig. S8). Earlier identifications of PBAP classes in Ny-Ålesund in two summers found very low concentrations of intact pollen and found local species to dominate over exotic pollen (Johansen and Hafsten, 1988), although sediment cores from Svalbard indicate considerable variability in the remote transport of exotic pollen (Poliakova et al., 2024). These earlier assessments also found a near constant presence of airborne fungal spores at considerable concentrations in Ny-Ålesund (Johansen and Hafsten, 1988), which is consistent with the prevalence of fungal spores identified by our classifier and the analyses of Freitas et al. (2023a) and Tobo et al. (2024).

Figure 7d reveals that the untuned dust LRM is also insensitive to variability in SSA and dust tracers, indicated by the near-constant, high fraction (∼80%) of particles labeled as dust. This high of a dust fraction is unlikely, since total coarse-mode particle concentrations measured by the MBS are strongly correlated with SSA tracers sodium, chloride, and magnesium, and do not correlate with mineral dust tracers (Fig. 7e). The modest but significant correlation between calcium and potassium with total coarse-mode particle concentrations may reflect that both marine and terrestrial sources can influence calcium aerosol content (Salter et al., 2016; Su et al., 2023; Solomon et al., 1989), and that potassium may be emitted by mineral dust, marine, and BB sources (Andreae, 1983). Inspecting non-fluorescent particles measured at Zeppelin Observatory during a sampling period with minimal dust influence (the minimum in silicon concentrations over 2020) reveals that they resembled dust more than SSA in laboratory characterization data (Fig. S6), suggesting that natural processes (e.g., aging of SSA) may have modified particle morphology. Karlsson et al. (2020) found similar difficulties in correctly identifying out-of-sample lab-generated SSA particles using conformal prediction. Laboratory-generated SSA properties vary markedly depending on generation method (e.g. Salter et al. 2015 and Christiansen et al. 2019), introducing biases to inductive approaches based on laboratory data.

To address this weakness, we applied domain adaptation on the dust LRM, this time using mineral constituents silicon, aluminum, iron, manganese, titanium, nickel, and chromium for mineral dust mass and the sum of major SSA ions (sodium, chloride, magnesium, and potassium) for sea spray; details of our dust influence metric's construction are further explained in the SI. This step's aim is to relax the dust LRM's fit on the highly regular scattering signatures of nascent laboratory-generated SSA described in Section 3.1 around Fig. 4. The tuning block's influence was again weighted according to our confidence in the field label based on a dust influence metric and on a scaling factor limiting the total influence of the tuning block on the LRM's training to 20% of that of the laboratory training data. The model's overall precision in identifying dust and SSA in laboratory data in r epeated in-sample testing was not significantly affected by the tuning (Fig. S9). Tuning the dust model significantly reduced the fraction of particles observed at Zeppelin Observatory classified as dust and increased dust fraction variability (Fig. 7d). The tuned model's resulting dust fraction was lowest when silicon concentrations were lowest between March-April, and increased episodically to maxima of ∼0.6 during summer when sodium concentrations were lowest. This results in a significant positive correlation with silicon and anti-correlation with SSA tracers sodium, chloride, and magnesium. These correlations are stronger than those from the untuned model's output (Fig. S7b). These fractions are consistent with those determined in this size range by Tobo et al. (2024) via electron microscopy (their Fig. 5a), who found that mineral dust particles comprised about half of particles >2 µm in March and July. A significant proportion of the remainder were mixed sea salt-mineral particles (Tobo et al., 2024); what scattering signatures these mixed particles would exhibit is unknown.

https://doi.org/10.5194/egusphere-2026-59
Preprint. Discussion started: 28 January 2026

4 Discussion

UV-LIF spectroscopy is a powerful tool for detecting bioaerosols, resolving single-particle fluorescence spectra and morphology at high frequency. We characterized common coarse-mode aerosol types in the laboratory, including pollen, bacteria, dust, and potential interferents like microplastics, producing a reference dataset for the MBS. These characterizations clarify what to expect when interpreting ambient measurements and differentiating PBAPs from interfering fluorescent materials. The pollen types assessed showed broadly consistent features, but with strong differences depending on nebulization method. Wet-nebulized pollen particles exhibited broader spectra and with peaks shifted towards the channel centered at 461 nm (wet) from that centered at 414 nm (dry). This suggests that hydration, cloud processing, or surface wetting can substantially modify pollen fluorescence, with implications for their identification in ambient observations. However, since the MBS can only detect SPPs and not intact pollen grains, wet-processed pollen samples are useful for understanding SPPs, which are primarily generated in humid conditions. This may be especially useful for detecting cloud-activated pollen fragments sampled via, e.g. counterflow virtual impactor (CVI) inlets (Freitas et al., 2024). As a complicating factor, pollen rupture is stochastic causing high variability in SPP morphologies, reflected in the wide range of scattering signatures we observed.

Fluorescence spectra of both PE and cellulose closely resemble those of pollen particles, posing potential challenges for pollen particle identification. Bacteria cultured from Baltic seawater exhibited fluorescence spectra consistent with previous measurements of marine bacteria and were clearly distinguishable from pollen, cellulose, and microplastics. Dust samples contained a small fraction ($\sim$10%) of weakly fluorescent particles, indicating the presence of some organic matter, potentially humic substances (Pöhlker et al., 2012). This feature may be useful in investigating atmospheric interactions such as ice nucleation, which humic substances have been posited to promote (Tobo et al., 2014; Chen et al., 2021; Pereira et al., 2022), but its exploitation is complicated in practice by interference from, e.g., coating by PAHs. We also compared our results with previously published MBS characterization studies of particles including bacteria, fungal spores, diesel engine combustion particles, and SSA. Notably, combustion particles showed broad fluorescence spectra similar to those of pollen and fungal spores with generally substantially stronger intensities, posing a major challenge in UV-LIF-based PBAP detection. Fungal spore and bacterial spectra shared strong similarities, complicating fPBAP class-specific identification. Dust particles exhibited distinct scattering properties, indicating higher asymmetry and irregular, rough surfaces than SSA.

We demonstrated the training of ML models on the combined body of MBS source experiment data using UMAP dimensionality reduction and k-nearest neighbors. In in-sample testing, the classifier displayed confusion between bacteria and fungal spores, and between pollen and fungal spores. Problematically, the multiclass fluorescent particle classifier misidentified $\sim$12% of combustion particles as pollen. For more robust filtering, we trained a separate binary classifier using logistic regression for flagging particles as pollution with the same training data, which performed better at distinguishing interferents from fluorescent PBAPs. Combining these two methods provides flexibility and builds redundancy into the classifier. The ease of tuning the LRM allowed us to implement domain adaptation using field validation data, improving correlations between our algorithm's fPBAP estimates and PBAP tracer concentrations. The significant correlation between the wood pyrolysis tracer levoglucosan and HFP concentrations indicates that particles originating from BB were likely misidentified as fPBAP by the untuned clas-

https://doi.org/10.5194/egusphere-2026-59
Preprint. Discussion started: 28 January 2026

sifier. These may differ from diesel engine-sourced combustion particles such as those included in our training data and could have been modified by aging processes. However, wildfires have been found to directly promote PBAP emissions (Moore et al., 2020; Kobziar et al., 2022; Ellington et al., 2024). Determining the degree to which biological tracer concentrations are influenced by, e.g., plant debris and PBAPs emitted via BB is ultimately difficult. Our classification algorithm may be improved in the future by including source characterization data from wood and biomass burning experiments.

Our classifier identified pollen and fungal spores as the most common classes of fPBAP observed at Zeppelin Observatory in 2020. While previous work establishes fungal spores as common in Ny-Ålesund (Johansen and Hafsten, 1988; Freitas et al., 2023a; Tobo et al., 2024), pollen concentrations were very low ($O(10^{-3})$ L^{-1} in summer) in past measurements (Johansen and Hafsten, 1988). However, SPP concentrations are difficult to estimate due to high variability in their emissions (Suphioglu et al., 1992; Subba et al., 2021) and difficulty in identifying them, making it challenging to verify their presence. Because the fluorescence spectra of pure cellulose closely resembled those of pollen and fungal spores, it is likely that some fPBAP identified by our classifier were misclassified plant debris. Since real plant debris was missing from the characterization data presented here, representing a potentially important missing class, we suggest that future characterizations measuring, e.g., leaf litter be conducted with the MBS to improve identification. Additional tracers could help verify class contributions to fPBAP detected by our classification algorithm, but source overlap complicates tracer interpretation. More source-specific tracers, such as sucrose for pollen (Mampage et al., 2022), dipicolinic acid for bacteria (Mampage et al., 2022), and ergosterol for fungal spores (Lau et al., 2006), are necessary to thoroughly validate fPBAP class contributions. Future assessments for specific fPBAP class validations when e.g., pollen trap counts, digital holography-based pollen identification, and aerobiome DNA sequencing are conducted in parallel to MBS observations should be made to provide further validation.

Finally, we trained another LRM to distinguish between larger (>2.5 µm) dust and SSA particles based only on optical scattering signatures. The dust model likely misidentified a large portion of extant particles observed at Zeppelin Observatory in this size range as dust despite high correlations between total coarse-mode particle concentrations and SSA tracers. Optical morphology signatures of ambient non-fluorescent particles in a period with minimal dust influence were more similar to those measured in dust rather than SSA characterization experiments (Figure S6). This suggests that nascent laboratory-generated SSA may not fully resemble naturally aged SSA or that the generation method biases certain particle morphologies, which are diverse in SSA (Salter et al., 2014; Christiansen et al., 2019). This may affect non-fluorescent particle identification in humid and cloudy conditions, since wet-processed SSA particles would undergo drying after sampling, or introduce sensitivity to humid measurement conditions in the instrument. Further study on how optical morphology properties measured with the MBS are affected by different aerosol generation methods (e.g. different SSA simulation chamber configurations) and aging processes could help improve particle identification and our interpretations of these optical morphology parameters. While optical methods for detecting irregular and asymmetric particle morphologies are commonly employed to estimate dust influence (Moosmüller et al., 2009), the MBS resolves single-particle morphology via optical diffraction, providing new opportunities for particle characterization and process study. Although the MBS's optics have been employed to distinguish between cloud droplets and ice crystals (Mahrt et al., 2019), our algorithm represents the first implication of these methods in identifying the most common inorganic coarse-mode aerosol types with its detection capabilities.

https://doi.org/10.5194/egusphere-2026-59
Preprint. Discussion started: 28 January 2026

5 Conclusions

Although UV-LIF spectroscopy allows for rapid online detection, characterization, and quantification of fluorescent PBAPs, interference from non-biological particle types must be considered. Here we present a new laboratory dataset characterizing pollen, bacteria, microplastic, cellulose, and dust particles using a UV-LIF instrument, and compare it with previously published experiments using the same instrument. We show that biological and non-biological particles can share fluorescence features that bias fluorescence-only classification approaches, and demonstrate how optical scattering-derived morphology information helps distinguish among fluorescent and non-fluorescent particle types. Using the combined fluorescence and morphology characterization data, we developed a particle classification algorithm using supervised ML trained on known particle types and applied it to one year of field observations from the Zeppelin Observatory, Svalbard. Compared to the previously validated fluorescence-only approach of (Freitas et al., 2023a), our algorithm yields up to an order of magnitude higher fluorescent PBAP concentrations during summer while preserving comparable correlations with PBAP molecular tracers. The main advantages of the ML-based classification algorithm for identifying fluorescent PBAPs are: i) explicit use of morphology for particle identification, which fluorescence-only approaches ignore; ii) broader classes of PBAPs, such as pollen particles; and iii) accounting for key interferents that can bias PBAP detection. Nevertheless, our results suggest that both our ML-based and fluorescence-only methods for classifying fluorescent PBAPs remain sensitive to interference from combustion particles. Our ML models were likely constrained by limited woodsmoke representation in the training datasets, which we partly mitigated through transfer learning using field-observed fluorescent particles and independent indicators of biological and pollution influence. Future work should expand source characterization data to include a wider array of combustion particles. It is unlikely that any classification scheme or instrument configuration will fully eliminate the influence of interferents, highlighting the need for parallel observations of e.g. black/brown carbon, pollen grains, and source-specific tracers for validating fluorescent PBAP quantifications. Despite site-specific variability in aerobiomes and fluorescence signatures, this framework provides a general, flexible approach for estimating PBAP concentrations across environments. Re-analyzing earlier MBS datasets with this algorithm can revise fluorescent PBAP estimates and test past conclusions using an independent identification strategy for both PBAPs and interferents. In addition, we implemented a dust detection component in our classification algorithm by exploiting optical morphology differences between dust and SSA, which can be used to help determine marine and terrestrial aerosol source influence in ambient observations. This algorithm can be redefined and improved as additional source experiment data characterizing other particle types and using more realistic emission pathways become available.

Code and data availability. The code used to reproduce these results and the classifier algorithm can be found at https://github.com/SU-air, and the data produced in this study is hosted at the Bolin Centre for Climate Research's database at ://bolin.su.se/data/jonsson-2025-wffj1j-1 (Jönsson et al., 2026). The data for Freitas et al. (2023a) can be found at the Bolin Centre Database at https://bolin.su.se/data/zeppelin-freitas-2023-bioaerosols-1 (Freitas et al., 2023b). Zeppelin Observatory tracer data (Yttri, 2023; Aas, 2024, 2025; Calzolai, 2025) used in this study were accessed from EBAS (https://ebas.nilu.no), hosted by NILU. Specifically, the use included data affiliated with the frameworks: ACTRIS, GAW-WDCA, GAW-WDCRG, CAMP, AMAP, NILU, and EMEP.

https://doi.org/10.5194/egusphere-2026-59
Preprint. Discussion started: 28 January 2026

Author contributions. We follow the Contributor Role Taxonomy (CRediT; https://credit.niso.org/). A.J.: Validation, Software, Methodology, Investigation, Formal analysis, Data curation, Visualization, Writing - Original Draft, Writing - Review & Editing; J.F.: Methodology, Investigation, Formal analysis, Data curation, Visualization, Writing - Review & Editing, Resources, Validation; G.F.: Software, Methodology, Investigation, Formal analysis, Data curation, Writing - Review & Editing, Validation; I.C.: Resources, Writing - Review & Editing, Data curation; P.D.-W.: Resources, Writing - Review & Editing; R.K.: Resources, Writing - Review & Editing, Data curation; Y.T.: Resources, Writing - Review & Editing; K.E.Y.: Resources, Writing - Review & Editing, Data curation; P.Z.: Conceptualization, Data curation, Funding acquisition, Investigation, Methodology, Project administration, Resources, Supervision, Writing - Review & Editing, Validation.

Competing interests. PZ and RK are co-editors at ACP.

Acknowledgements. This work was funded by the European Union's Horizon Europe Programme under Grant Agreement No. 101137639 (CleanCloud), and supported by the Swedish Research Council (grant no. 2018-05045) and Swedish Environmental Protection Agency (Naturvårdsverket). We are thankful to Zbynek Drab and Pharmallerga CZ S.r.o. for providing pollen samples and analyses, Julika Zinke and the Baltic Sea Centre for providing bacterial cultures, Elena Gorokhova (Department of Environmental Science, Stockholm University) for providing PE and cellulose samples, Ingrid Zieger for providing the Sakurajima dust sample, Birgitta Liewenborg (Department of Environmental Science, Stockholm University) for providing the clay dust sample, and David Topping (Centre for Atmospheric Science, University of Manchester) for providing the MBS data obtained in Ruske et al. (2017). Observations at Zeppelin Observatory were supported by the Swedish Environmental Protection Agency (Naturvårdsverket), Knut and Alice Wallenberg Foundation (Knut och Alice Wallenbergs Stiftelse; KAW) ACAS project grant no. 2016.0024, and by ACTRIS-Sweden. The authors wish to acknowledge the support and collaboration of the University of Hertfordshire, particularly Paul Kaye and Warren Stanley, in the development and maintenance of the MBS instrument.

https://doi.org/10.5194/egusphere-2026-59
Preprint. Discussion started: 28 January 2026

References

Aas, W.: CAMP, NILU, EMEP, AMAP, 2017-2025, Heavy metals at Zeppelin mountain (Ny-Ålesund), data hosted by EBAS at NILU, https://doi.org/10.48597/6PXH-3ESD, accessed 2025-8-11, 2024.

Aas, W.: EMEP, CAMP, NILU, AMAP, 2001-2025, Inorganics in air and particle phase at Zeppelin mountain (Ny-Ålesund), data hosted by EBAS at NILU, https://doi.org/10.48597/H7PV-77C5, accessed 2025-6-16, 2025.

Adebiyi, A., Kok, J. F., Murray, B. J., Ryder, C. L., Stuut, J.-B. W., Kahn, R. A., Knippertz, P., Formenti, P., Mahowald, N. M., Pérez García-Pando, C., Klose, M., Ansmann, A., Samset, B. H., Ito, A., Balkanski, Y., Di Biagio, C., Romanias, M. N., Huang, Y., and Meng, J.: A review of coarse mineral dust in the Earth system, Aeolian Research, 60, 100 849, https://doi.org/10.1016/j.aeolia.2022.100849, 2023.

Andreae, M. O.: Soot Carbon and Excess Fine Potassium: Long-Range Transport of Combustion-Derived Aerosols, Science, 220, 1148–1151, https://doi.org/10.1126/science.220.4602.1148, 1983.

Andreae, M. O. and Gelencsér, A.: Black carbon or brown carbon? The nature of light-absorbing carbonaceous aerosols, Atmospheric Chemistry and Physics, 6, 3131–3148, https://doi.org/10.5194/acp-6-3131-2006, 2006.

Arnalds, O., Dagsson-Waldhauserova, P., and Olafsson, H.: The Icelandic volcanic aeolian environment: Processes and impacts — A review, Aeolian Research, 20, 176–195, https://doi.org/10.1016/j.aeolia.2016.01.004, 2016.

Bai, X., Luo, L., Tian, H., Liu, S., Hao, Y., Zhao, S., Lin, S., Zhu, C., Guo, Z., and Lv, Y.: Atmospheric Vanadium Emission Inventory from Both Anthropogenic and Natural Sources in China, Environmental Science & Technology, 55, 11 568–11 578, https://doi.org/10.1021/acs.est.1c04766, 2021.

Bauer, H., Claeys, M., Vermeylen, R., Schueller, E., Weinke, G., Berger, A., and Puxbaum, H.: Arabitol and mannitol as tracers for the quantification of airborne fungal spores, Atmospheric Environment, 42, 588–593, https://doi.org/10.1016/j.atmosenv.2007.10.013, 2008.

Beck, I., Moallemi, A., Heutte, B., Pernov, J. B., Bergner, N., Rolo, M., Quéléver, L. L. J., Laurila, T., Boyer, M., Jokinen, T., Angot, H., Hoppe, C. J. M., Müller, O., Creamean, J., Frey, M. M., Freitas, G., Zinke, J., Salter, M., Zieger, P., Mirrielees, J. A., Kempf, H. E., Ault, A. P., Pratt, K. A., Gysel-Beer, M., Henning, S., Tatzelt, C., and Schmale, J.: Characteristics and sources of fluorescent aerosols in the central Arctic Ocean, Elementa: Science of the Anthropocene, 12, 00 125, https://doi.org/10.1525/elementa.2023.00125, 2024.

Bertram, T. H., Cochran, R. E., Grassian, V. H., and Stone, E. A.: Sea spray aerosol chemical composition: elemental and molecular mimics for laboratory studies of heterogeneous and multiphase reactions, Chem. Soc. Rev., 47, 2374–2400, https://doi.org/10.1039/C7CS00008A, 2018.

Bozzetti, C., Daellenbach, K. R., Hueglin, C., Fermo, P., Sciare, J., Kasper-Giebl, A., Mazar, Y., Abbaszade, G., El Kazzi, M., Gonzalez, R., Shuster-Meiseles, T., Flasch, M., Wolf, R., Křepelová, A., Canonaco, F., Schnelle-Kreis, J., Slowik, J. G., Zimmermann, R., Rudich, Y., Baltensperger, U., El Haddad, I., and Prévôt, A. S. H.: Size-Resolved Identification, Characterization, and Quantification of Primary Biological Organic Aerosol at a European Rural Site, Environmental Science & Technology, 50, 3425–3434, https://doi.org/10.1021/acs.est.5b05960, 2016.

Calzolai, G.: NILU, 2017-2020, Heavy metals, inorganics in air and particle phase, silicon and sulphur at Zeppelin mountain (Ny-Ålesund), data hosted by EBAS at NILU, https://doi.org/10.48597/8SEU-C5UP, accessed 2025-8-12, 2025.

Chen, J., Wu, Z. J., Zhao, X., Wang, Y. J., Chen, J. C., Qiu, Y. T., Zong, T. M., Chen, H. X., Wang, B. B., Lin, P., Liu, W., Guo, S., Yao, M. S., Zeng, L. M., Wex, H., Liu, X., Hu, M., and Li, S. M.: Atmospheric Humic-Like Substances (HULIS) Act as Ice Active Entities, Geophysical Research Letters, 48, e2021GL092 443, https://doi.org/10.1029/2021GL092443, e2021GL092443 2021GL092443, 2021.

https://doi.org/10.5194/egusphere-2026-59
Preprint. Discussion started: 28 January 2026

China, S., Wang, B., Weis, J., Rizzo, L., Brito, J., Cirino, G. G., Kovarik, L., Artaxo, P., Gilles, M. K., and Laskin, A.: Rupturing of Biological Spores As a Source of Secondary Particles in Amazonia, Environmental Science & Technology, 50, 12 179–12 186, https://doi.org/10.1021/acs.est.6b02896, 2016.

Choobari, O. A., Zawar-Reza, P., and Sturman, A.: The global distribution of mineral dust and its impacts on the climate system: A review, Atmospheric Research, 138, 152–165, https://doi.org/10.1016/j.atmosres.2013.11.007, 2014.

Christiansen, S., Salter, M. E., Gorokhova, E., Nguyen, Q. T., and Bilde, M.: Sea Spray Aerosol Formation: Laboratory Results on the Role of Air Entrainment, Water Temperature, and Phytoplankton Biomass, Environmental Science & Technology, 53, 13 107–13 116, https://doi.org/10.1021/acs.est.9b04078, 2019.

Clarke, K. R.: Non-parametric multivariate analyses of changes in community structure, Australian Journal of Ecology, 18, 117–143, https://doi.org/10.1111/j.1442-9993.1993.tb00438.x, 1993.

Conen, F. and Yakutin, M. V.: Soils rich in biological ice-nucleating particles abound in ice-nucleating macromolecules likely produced by fungi, Biogeosciences, 15, 4381–4385, https://doi.org/10.5194/bg-15-4381-2018, 2018.

Crawford, I., Ruske, S., Topping, D. O., and Gallagher, M. W.: Evaluation of hierarchical agglomerative cluster analysis methods for discrimination of primary biological aerosol, Atmospheric Measurement Techniques, 8, 4979–4991, https://doi.org/10.5194/amt-8-4979-2015, 2015.

Crawford, I., Topping, D., Gallagher, M., Forde, E., Lloyd, J. R., Foot, V., Stopford, C., and Kaye, P.: Detection of Airborne Biological Particles in Indoor Air Using a Real-Time Advanced Morphological Parameter UV-LIF Spectrometer and Gradient Boosting Ensemble Decision Tree Classifiers, Atmosphere, 11, https://doi.org/10.3390/atmos11101039, 2020.

Crawford, I., Bower, K., Topping, D., Di Piazza, S., Massabò, D., Vernocchi, V., and Gallagher, M.: Towards a UK Airborne Bioaerosol Climatology: Real-Time Monitoring Strategies for High Time Resolution Bioaerosol Classification and Quantification, Atmosphere, 14, https://doi.org/10.3390/atmos14081214, 2023.

Crawford, J., Cohen, D. D., Chambers, S. D., Williams, A. G., and Atanacio, A.: Impact of aerosols of sea salt origin in a coastal basin: Sydney, Australia, Atmospheric Environment, 207, 52–62, https://doi.org/10.1016/j.atmosenv.2019.03.018, 2019.

Després, V. R., Huffman, J. A., Burrows, S. M., Hoose, C., Safatov, A. S., Buryak, G., Fröhlich-Nowoisky, J., Elbert, W., Andreae, M. O., Pöschl, U., and Jaenicke, R.: Primary biological aerosol particles in the atmosphere: a review, Tellus B: Chemical and Physical Meteorology, 64, 15 598, https://doi.org/10.3402/tellusb.v64i0.15598, 2012.

Di Filippo, P., Pomata, D., Riccardi, C., Buiarelli, F., and Perrino, C.: Fungal contribution to size-segregated aerosol measured through biomarkers, Atmospheric Environment, 64, 132–140, https://doi.org/10.1016/j.atmosenv.2012.10.010, 2013.

El Morr, C., Jammal, M., Ali-Hassan, H., and El-Hallak, W.: Logistic Regression, pp. 231–249, Springer International Publishing, Cham, https://doi.org/10.1007/978-3-031-16990-8_7, 2022.

Ellington, A. J., Walters, K., Christner, B. C., Fox, S., Bonfantine, K., Walker, C., Lampman, P., Vuono, D. C., Strickland, M., Lambert, K., and Kobziar, L. N.: Dispersal of microbes from grassland fire smoke to soils, The ISME Journal, 18, wrae203, https://doi.org/10.1093/ismejo/wrae203, 2024.

Fang, K., Wang, Y., Yu, T., Zhang, L., Baluška, F., Šamaj, J., and Lin, J.: Isolation of de-exined pollen and cytological studies of the pollen intines of Pinus bungeana Zucc. Ex Endl. and Picea wilsonii Mast, Flora - Morphology, Distribution, Functional Ecology of Plants, 203, 332–340, https://doi.org/10.1016/j.flora.2007.04.007, 2008.

Fennelly, M. J., Sewell, G., Prentice, M. B., O'Connor, D. J., and Sodeau, J. R.: Review: The Use of Real-Time Fluorescence Instrumentation to Monitor Ambient Primary Biological Aerosol Particles (PBAP), Atmosphere, 9, https://doi.org/10.3390/atmos9010001, 2018.

https://doi.org/10.5194/egusphere-2026-59
Preprint. Discussion started: 28 January 2026

Freitas, G. P., Stolle, C., Kaye, P. H., Stanley, W., Herlemann, D. P. R., Salter, M. E., and Zieger, P.: Emission of primary bioaerosol particles from Baltic seawater, Environmental Science: Atmospheres, 2, 1170–1182, https://doi.org/10.1039/d2ea00047d, 2022.

Freitas, G. P., Adachi, K., Conen, F., Heslin-Rees, D., Krejci, R., Tobo, Y., Yttri, K. E., and Zieger, P.: Regionally sourced bioaerosols drive high-temperature ice nucleating particles in the Arctic, Nature Communications, 14, 5997, https://doi.org/10.1038/s41467-023-41696-7, 2023a.

Freitas, G. P., Conen, F., Adachi, K., Yttri, K. E., Krejci, R., and Zieger, P.: Concentration of bioaerosols and ice nucleating particles at Zeppelin Observatory, Svalbard, 2017-2020, Dataset version 1. Bolin Centre Database., https://doi.org/10.17043/zeppelin-freitas-2023-bioaerosols-1, accessed: 2025-07-09, 2023b.

Freitas, G. P., Kopec, B., Adachi, K., Krejci, R., Heslin-Rees, D., Yttri, K. E., Hubbard, A., Welker, J. M., and Zieger, P.: Contribution of fluorescent primary biological aerosol particles to low-level Arctic cloud residuals, Atmospheric Chemistry and Physics, 24, 5479–5494, https://doi.org/10.5194/acp-24-5479-2024, 2024.

Fu, Y. and Finney, N. S.: Small-molecule fluorescent probes and their design, RSC Adv., 8, 29 051–29 061, https://doi.org/10.1039/C8RA02297F, 2018.

Gantt, E. and Cunningham Jr, F. X.: Algal Pigments, John Wiley & Sons, Ltd, https://doi.org/10.1038/npg.els.0000323, 2001.

Gao, K., Vogel, F., Foskinis, R., Vratolis, S., Gini, M. I., Granakis, K., Billault-Roux, A.-C., Georgakaki, P., Zografou, O., Fetfatzis, P., Berne, A., Papayannis, A., Eleftheridadis, K., Möhler, O., and Nenes, A.: Biological and dust aerosols as sources of ice-nucleating particles in the eastern Mediterranean: source apportionment, atmospheric processing and parameterization, Atmospheric Chemistry and Physics, 24, 9939–9974, https://doi.org/10.5194/acp-24-9939-2024, 2024.

Gill, T. E., Zobeck, T. M., and Stout, J. E.: Technologies for laboratory generation of dust from geological materials, Journal of Hazardous Materials, 132, 1–13, https://doi.org/10.1016/j.jhazmat.2005.11.083, generation and Control of Hazardous Dusts from Geologic Media, 2006.

Gliß, J., Mortier, A., Schulz, M., Andrews, E., Balkanski, Y., Bauer, S. E., Benedictow, A. M. K., Bian, H., Checa-Garcia, R., Chin, M., Ginoux, P., Griesfeller, J. J., Heckel, A., Kipling, Z., Kirkevåg, A., Kokkola, H., Laj, P., Le Sager, P., Lund, M. T., Lund Myhre, C., Matsui, H., Myhre, G., Neubauer, D., van Noije, T., North, P., Olivié, D. J. L., Rémy, S., Sogacheva, L., Takemura, T., Tsigaridis, K., and Tsyro, S. G.: AeroCom phase III multi-model evaluation of the aerosol life cycle and optical properties using ground- and space-based remote sensing as well as surface in situ observations, Atmospheric Chemistry and Physics, 21, 87–128, https://doi.org/10.5194/acp-21-87-2021, 2021.

Gosselin, M. I., Rathnayake, C. M., Crawford, I., Pöhlker, C., Fröhlich-Nowoisky, J., Schmer, B., Després, V. R., Engling, G., Gallagher, M., Stone, E., Pöschl, U., and Huffman, J. A.: Fluorescent bioaerosol particle, molecular tracer, and fungal spore concentrations during dry and rainy periods in a semi-arid forest, Atmospheric Chemistry and Physics, 16, 15 165–15 184, https://doi.org/10.5194/acp-16-15165-2016, 2016.

Gratzl, J., Seifried, T. M., Stolzenburg, D., and Grothe, H.: A fluorescence approach for an online measurement technique of atmospheric microplastics, Environ. Sci.: Atmos., 4, 601–610, https://doi.org/10.1039/D4EA00010B, 2024.

Hartmann, S., Schrödner, R., Hassett, B. T., Hartmann, M., van Pinxteren, M., Fomba, K. W., Stratmann, F., Herrmann, H., Pöhlker, M., and Zeppenfeld, S.: Polysaccharides – Important Constituents of Ice-Nucleating Particles of Marine Origin, Environmental Science & Technology, 59, 5098–5108, https://doi.org/10.1021/acs.est.4c08014, 2025.

Healy, J. and McInnes, L.: Uniform manifold approximation and projection, Nature Reviews Methods Primers, 4, 82, https://doi.org/10.1038/s43586-024-00363-x, 2024.

https://doi.org/10.5194/egusphere-2026-59
Preprint. Discussion started: 28 January 2026

Hess, M. W.: Cell-wall development in freeze-fixed pollen: Intine formation of Ledebouria socialis (Hyacinthaceae), Planta, 189, 139–149, https://doi.org/10.1007/BF00201354, 1993.

Hiranuma, N., Möhler, O., Yamashita, K., Tajiri, T., Saito, A., Kiselev, A., Hoffmann, N., Hoose, C., Jantsch, E., Koop, T., and Murakami, M.: Ice nucleation by cellulose and its potential contribution to ice formation in clouds, Nature Geoscience, 8, 273–277, https://doi.org/10.1038/ngeo2374, 2015.

Hiranuma, N., Adachi, K., Bell, D. M., Belosi, F., Beydoun, H., Bhaduri, B., Bingemer, H., Budke, C., Clemen, H.-C., Conen, F., Cory, K. M., Curtius, J., DeMott, P. J., Eppers, O., Grawe, S., Hartmann, S., Hoffmann, N., Höhler, K., Jantsch, E., Kiselev, A., Koop, T., Kulkarni, G., Mayer, A., Murakami, M., Murray, B. J., Nicosia, A., Petters, M. D., Piazza, M., Polen, M., Reicher, N., Rudich, Y., Saito, A., Santachiara, G., Schiebel, T., Schill, G. P., Schneider, J., Segev, L., Stopelli, E., Sullivan, R. C., Suski, K., Szakáll, M., Tajiri, T., Taylor, H., Tobo, Y., Ullrich, R., Weber, D., Wex, H., Whale, T. F., Whiteside, C. L., Yamashita, K., Zelenyuk, A., and Möhler, O.: A comprehensive characterization of ice nucleation by three different types of cellulose particles immersed in water, Atmospheric Chemistry and Physics, 19, 4823–4849, https://doi.org/10.5194/acp-19-4823-2019, 2019.

Hird, C., Perron, M. M. G., Holmes, T. M., Meyerink, S., Nielsen, C., Townsend, A. T., de Caritat, P., Strzelec, M., and Bowie, A. R.: On the use of lithogenic tracer measurements in aerosols to constrain dust deposition fluxes to the ocean southeast of Australia, Aerosol Research, 2, 315–327, https://doi.org/10.5194/ar-2-315-2024, 2024.

Holden, A. S., Sullivan, A. P., Munchak, L. A., Kreidenweis, S. M., Schichtel, B. A., Malm, W. C., and Collett, J. L.: Determining contributions of biomass burning and other sources to fine particle contemporary carbon in the western United States, Atmospheric Environment, 45, 1986–1993, https://doi.org/10.1016/j.atmosenv.2011.01.021, 2011.

Hoose, C. and Möhler, O.: Heterogeneous ice nucleation on atmospheric aerosols: a review of results from laboratory experiments, Atmospheric Chemistry and Physics, 12, 9817–9854, https://doi.org/10.5194/acp-12-9817-2012, 2012.

Huang, S., Hu, W., Chen, J., Wu, Z., Zhang, D., and Fu, P.: Overview of biological ice nucleating particles in the atmosphere, Environment International, 146, 106 197, https://doi.org/10.1016/j.envint.2020.106197, 2021.

Huffman, J. A., Perring, A. E., Savage, N. J., Clot, B., Crouzy, B., Tummon, F., Shoshanim, O., Damit, B., Schneider, J., Sivaprakasam, V., Zawadowicz, M. A., Crawford, I., Gallagher, M., Topping, D., Doughty, D. C., Hill, S. C., and and, Y. P.: Real-time sensing of bioaerosols: Review and current perspectives, Aerosol Science and Technology, 54, 465–495, https://doi.org/10.1080/02786826.2019.1664724, 2020.

Hughes, D. D., Mampage, C. B. A., Jones, L. M., Liu, Z., and Stone, E. A.: Characterization of Atmospheric Pollen Fragments during Springtime Thunderstorms, Environmental Science & Technology Letters, 7, 409–414, https://doi.org/10.1021/acs.estlett.0c00213, 2020.

Jacquot, J. L., Shen, X., Abou-Ghanem, M., Froyd, K. D., Lawler, M., Schill, G. P., Slovacek, K., Thomson, D. S., Cziczo, D. J., and Murphy, D. M.: A new airborne single particle mass spectrometer: PALMS-NG, Aerosol Science and Technology, 58, 991–1007, https://doi.org/10.1080/02786826.2024.2331549, 2024.

Jia, W., Sun, M., Lian, J., and Hou, S.: Feature dimensionality reduction: a review, Complex & Intelligent Systems, 8, 2663–2693, https://doi.org/10.1007/s40747-021-00637-x, 2022.

Jia, Y. and Fraser, M.: Characterization of Saccharides in Size-fractionated Ambient Particulate Matter and Aerosol Sources: The Contribution of Primary Biological Aerosol Particles (PBAPs) and Soil to Ambient Particulate Matter, Environmental Science & Technology, 45, 930–936, https://doi.org/10.1021/es103104e, 2011.

Jia, Y., Bhat, S., and Fraser, M. P.: Characterization of saccharides and other organic compounds in fine particles and the use of saccharides to track primary biologically derived carbon sources, Atmospheric Environment, 44, 724–732, https://doi.org/10.1016/j.atmosenv.2009.10.034, 2010.

https://doi.org/10.5194/egusphere-2026-59
Preprint. Discussion started: 28 January 2026

Johansen, S. and Hafsten, U.: Airborne pollen and spore registrations at Ny-Ålesund, Svalbard, summer 1986, Polar Research, 6, 11–17, https://doi.org/10.1111/j.1751-8369.1988.tb00577.x, 1988.

Jönsson, A., Fu, J., Freitas, G. P., Zieger, P., and Crawford, I.: Multiparameter bioaerosol spectrometer (MBS) laboratory characterization experiments of coarse-mode particles, Dataset version 1. Bolin Centre Database., https://doi.org/10.17043/jonsson-2025-wffj1j-1, Submitted, 2026.

Kaluarachchi, C. P., Or, V. W., Lan, Y., Hasenecz, E. S., Kim, D., Madawala, C. K., Dorcé, G. P., Mayer, K. J., Sauer, J. S., Lee, C., Cappa, C. D., Bertram, T. H., Stone, E. A., Prather, K. A., Grassian, V. H., and Tivanski, A. V.: Effects of Atmospheric Aging Processes on Nascent Sea Spray Aerosol Physicochemical Properties, ACS Earth and Space Chemistry, 6, 2732–2744, https://doi.org/10.1021/acsearthspacechem.2c00258, 2022.

Karle, N. N., Sakai, R. K., Chiao, S., Fitzgerald, R. M., and Stockwell, W. R.: Reinterpreting Trends: The Impact of Methodological Changes on Reported Sea Salt Aerosol Levels, Atmosphere, 15, https://doi.org/10.3390/atmos15070740, 2024.

Karlsson, L., Boström, H., and Zieger, P.: Classication of aerosol particles using inductive conformal prediction, in: Proceedings of the Ninth Symposium on Conformal and Probabilistic Prediction and Applications, edited by Gammerman, A., Vovk, V., Luo, Z., Smirnov, E., and Cherubin, G., vol. 128 of *Proceedings of Machine Learning Research*, pp. 257–268, PMLR, 2020.

Karlsson, L., Baccarini, A., Duplessis, P., Baumgardner, D., Brooks, I. M., Chang, R. Y.-W., Dada, L., Dällenbach, K. R., Heikkinen, L., Krejci, R., Leaitch, W. R., Leck, C., Partridge, D. G., Salter, M. E., Wernli, H., Wheeler, M. J., Schmale, J., and Zieger, P.: Physical and Chemical Properties of Cloud Droplet Residuals and Aerosol Particles During the Arctic Ocean 2018 Expedition, Journal of Geophysical Research: Atmospheres, 127, e2021JD036 383, https://doi.org/10.1029/2021JD036383, e2021JD036383 2021JD036383, 2022.

Kobziar, L. N., Vuono, D., Moore, R., Christner, B. C., Dean, T., Betancourt, D., Watts, A. C., Aurell, J., and Gullett, B.: Wildland fire smoke alters the composition, diversity, and potential atmospheric function of microbial life in the aerobiome, ISME Communications, 2, 8, https://doi.org/10.1038/s43705-022-00089-5, 2022.

Kojoj, J., Freitas, G. P., Muilwijk, M., Granskog, M. A., Naakka, T., Ekman, A. M. L., Heutte, B., Schmale, J., Da Silva, A., Lapere, R., Marelle, L., Thomas, J. L., Melsheimer, C., Murray, B. J., and Zieger, P.: An Arctic Marine Source of Fluorescent Primary Biological Aerosol Particles During the Transition from Summer to Autumn at the North Pole, Tellus B: Chemical and Physical Meteorology, https://doi.org/10.16993/tellusb.1880, 2024.

Kulpinski, P., Erdman, A., Namyslak, M., and Fidelus, J. D.: Cellulose fibers modified by Eu3+-doped yttria-stabilized zirconia nanoparticles, Cellulose, 19, 1259–1269, https://doi.org/10.1007/s10570-012-9704-6, 2012.

Lai, S.-H., Maclot, S., Antoine, R., and Masselon, C. D.: Advances in Single Particle Mass Analysis, Mass Spectrometry Reviews, 44, 850–869, https://doi.org/10.1002/mas.21920, 2025.

Lau, A. P., Lee, A. K., Chan, C. K., and Fang, M.: Ergosterol as a biomarker for the quantification of the fungal biomass in atmospheric aerosols, Atmospheric Environment, 40, 249–259, https://doi.org/10.1016/j.atmosenv.2005.09.048, 2006.

Lee, H. D., Morris, H. S., Laskina, O., Sultana, C. M., Lee, C., Jayarathne, T., Cox, J. L., Wang, X., Hasenecz, E. S., DeMott, P. J., Bertram, T. H., Cappa, C. D., Stone, E. A., Prather, K. A., Grassian, V. H., and Tivanski, A. V.: Organic Enrichment, Physical Phase State, and Surface Tension Depression of Nascent Core-Shell Sea Spray Aerosols during Two Phytoplankton Blooms, ACS Earth and Space Chemistry, 4, 650–660, https://doi.org/10.1021/acsearthspacechem.0c00032, 2020.

Lu, D., Tan, J., Yang, X., Sun, X., Liu, Q., and Jiang, G.: Unraveling the role of silicon in atmospheric aerosol secondary formation: a new conservative tracer for aerosol chemistry, Atmospheric Chemistry and Physics, 19, 2861–2870, https://doi.org/10.5194/acp-19-2861-2019, 2019.

https://doi.org/10.5194/egusphere-2026-59
Preprint. Discussion started: 28 January 2026

Madawala, C. K., Molina, C., Kim, D., Gamage, D. K., Sun, M., Leibensperger III, R. J., Mehndiratta, L., Lee, J., Kaluarachchi, C. P., Kimble, K. A., Sandstrom, G., Harb, C., Dinasquet, J., Malfatti, F., Prather, K. A., Deane, G. B., Stokes, M. D., Lee, C., Slade, J. H., Stone, E. A., Grassian, V. H., and Tivanski, A. V.: Effects of Wind Speed on Size-Dependent Morphology and Composition of Sea Spray Aerosols, ACS Earth and Space Chemistry, 8, 1609–1622, https://doi.org/10.1021/acsearthspacechem.4c00119, 2024.

Mahrt, F., Wieder, J., Dietlicher, R., Smith, H. R., Stopford, C., and Kanji, Z. A.: A high-speed particle phase discriminator (PPD-HS) for the classification of airborne particles, as tested in a continuous flow diffusion chamber, Atmospheric Measurement Techniques, 12, 3183–3208, https://doi.org/10.5194/amt-12-3183-2019, 2019.

Maki, L. R., Galyan, E. L., Chang-Chien, M.-M., and Caldwell, D. R.: Ice Nucleation Induced by Pseudomonas syringae, Applied Microbiology, 28, 456–459, https://doi.org/10.1128/am.28.3.456-459.1974, 1974.

Mampage, C. B., Hughes, D. D., Jones, L. M., Metwali, N., Thorne, P. S., and Stone, E. A.: Characterization of subpollen particles in size-resolved atmospheric aerosol using chemical tracers, Atmospheric Environment: X, 15, 100 177, https://doi.org/10.1016/j.aeaoa.2022.100177, 2022.

Markey, E., Hourihane Clancy, J., Martínez-Bracero, M., Sarda-Estève, R., Baisnée, D., McGillicuddy, E. J., Sewell, G., Skjøth, C. A., and O'Connor, D. J.: Spectroscopic detection of bioaerosols with the WIBS-4+: Anthropogenic and meteorological impacts, Science of The Total Environment, 943, 173 649, https://doi.org/10.1016/j.scitotenv.2024.173649, 2024.

Matthews, B. H., Alsante, A. N., and Brooks, S. D.: Pollen Emissions of Subpollen Particles and Ice Nucleating Particles, ACS Earth and Space Chemistry, 7, 1207–1218, https://doi.org/10.1021/acsearthspacechem.3c00014, 2023.

McInnes, L., Healy, J., and Melville, J.: UMAP: Uniform Manifold Approximation and Projection for Dimension Reduction, https://arxiv.org/abs/1802.03426, 2020.

Medeiros, P. M., Conte, M. H., Weber, J. C., and Simoneit, B. R.: Sugars as source indicators of biogenic organic carbon in aerosols collected above the Howland Experimental Forest, Maine, Atmospheric Environment, 40, 1694–1705, https://doi.org/10.1016/j.atmosenv.2005.11.001, 2006.

Moore, R. A., Bomar, C., Kobziar, L. N., and Christner, B. C.: Wildland fire as an atmospheric source of viable microbial aerosols and biological ice nucleating particles, The ISME Journal, 15, 461–472, https://doi.org/10.1038/s41396-020-00788-8, 2020.

Moosmüller, H., Chakrabarty, R., and Arnott, W.: Aerosol light absorption and its measurement: A review, Journal of Quantitative Spectroscopy and Radiative Transfer, 110, 844–878, https://doi.org/10.1016/j.jqsrt.2009.02.035, light Scattering: Mie and More Commemorating 100 years of Mie's 1908 publication, 2009.

Morgana, S., Casentini, B., Tirelli, V., Grasso, F., and Amalfitano, S.: Fluorescence-based detection: A review of current and emerging techniques to unveil micro/ nanoplastics in environmental samples, TrAC Trends in Analytical Chemistry, 172, 117 559, https://doi.org/10.1016/j.trac.2024.117559, 2024.

Murray, B. J., O'Sullivan, D., Atkinson, J. D., and Webb, M. E.: Ice nucleation by particles immersed in supercooled cloud droplets, Chem. Soc. Rev., 41, 6519–6554, https://doi.org/10.1039/C2CS35200A, 2012.

Nash, D. G., Baer, T., and Johnston, M. V.: Aerosol mass spectrometry: An introductory review, International Journal of Mass Spectrometry, 258, 2–12, https://doi.org/10.1016/j.ijms.2006.09.017, aerosols/Microparticles Special Issue, 2006.

Nocedal, J.: Large-Scale Unconstrained Optimization, pp. 164–192, Springer New York, New York, NY, https://doi.org/10.1007/978-0-387-40065-5_7, 2006.

Pacini, E., Guarnieri, M., and Nepi, M.: Pollen carbohydrates and water content during development, presentation, and dispersal: a short review, Protoplasma, 228, 73–77, https://doi.org/10.1007/s00709-006-0169-z, 2006.

https://doi.org/10.5194/egusphere-2026-59
Preprint. Discussion started: 28 January 2026

Pandey, D., Banerjee, T., Badola, N., and Chauhan, J. S.: Evidences of microplastics in aerosols and street dust: a case study of Varanasi City, India, Environmental Science and Pollution Research, 29, 82 006–82 013, https://doi.org/10.1007/s11356-022-21514-1, 2022.

Pasquier, J. T., David, R. O., Freitas, G., Gierens, R., Gramlich, Y., Haslett, S., Li, G., Schäfer, B., Siegel, K., Wieder, J., Adachi, K., Belosi, F., Carlsen, T., Decesari, S., Ebell, K., Gilardoni, S., Gysel-Beer, M., Henneberger, J., Inoue, J., Kanji, Z. A., Koike, M., Kondo, Y., Krejci, R., Lohmann, U., Maturilli, M., Mazzolla, M., Modini, R., Mohr, C., Motos, G., Nenes, A., Nicosia, A., Ohata, S., Paglione, M., Park, S., Pileci, R. E., Ramelli, F., Rinaldi, M., Ritter, C., Sato, K., Storelvmo, T., Tobo, Y., Traversi, R., Viola, A., and Zieger, P.: The Ny-Ålesund Aerosol Cloud Experiment (NASCENT): Overview and First Results, Bulletin of the American Meteorological Society, 103, E2533 – E2558, https://doi.org/10.1175/BAMS-D-21-0034.1, 2022.

Pereira, D. L., Gavilán, I., Letechipía, C., Raga, G. B., Puig, T. P., Mugica-Álvarez, V., Alvarez-Ospina, H., Rosas, I., Martinez, L., Salinas, E., Quintana, E. T., Rosas, D., and Ladino, L. A.: Mexican agricultural soil dust as a source of ice nucleating particles, Atmospheric Chemistry and Physics, 22, 6435–6447, https://doi.org/10.5194/acp-22-6435-2022, 2022.

Platt, S. M., Hov, Ø., Berg, T., Breivik, K., Eckhardt, S., Eleftheriadis, K., Evangeliou, N., Fiebig, M., Fisher, R., Hansen, G., Hansson, H.-C., Heintzenberg, J., Hermansen, O., Heslin-Rees, D., Holmén, K., Hudson, S., Kallenborn, R., Krejci, R., Krognes, T., Larssen, S., Lowry, D., Lund Myhre, C., Lunder, C., Nisbet, E., Nizzetto, P. B., Park, K.-T., Pedersen, C. A., Aspmo Pfaffhuber, K., Röckmann, T., Schmidbauer, N., Solberg, S., Stohl, A., Ström, J., Svendby, T., Tunved, P., Tørnkvist, K., van der Veen, C., Vratolis, S., Yoon, Y. J., Yttri, K. E., Zieger, P., Aas, W., and Tørseth, K.: Atmospheric composition in the European Arctic and 30 years of the Zeppelin Observatory, Ny-Ålesund, Atmospheric Chemistry and Physics, 22, 3321–3369, https://doi.org/10.5194/acp-22-3321-2022, 2022.

Pöhlker, C., Huffman, J. A., and Pöschl, U.: Autofluorescence of atmospheric bioaerosols – fluorescent biomolecules and potential interferences, Atmospheric Measurement Techniques, 5, 37–71, https://doi.org/10.5194/amt-5-37-2012, 2012.

Poliakova, A., Brown, A. G., and Alsos, I. G.: Exotic pollen in sediments from the high Arctic Lake Tenndammen, Svalbard archipelago: diversity, sources, and transport pathways, Palynology, 48, 2287 005, https://doi.org/10.1080/01916122.2023.2287005, 2024.

Prank, M., Tonttila, J., Shang, X., Romakkaniemi, S., and Raatikainen, T.: Can pollen affect precipitation?, Atmospheric Chemistry and Physics, 25, 183–197, https://doi.org/10.5194/acp-25-183-2025, 2025.

Pratt, K. A. and Prather, K. A.: Mass spectrometry of atmospheric aerosols—Recent developments and applications. Part II: On-line mass spectrometry techniques, Mass Spectrometry Reviews, 31, 17–48, https://doi.org/10.1002/mas.20330, 2012.

Rathnayake, C. M., Metwali, N., Jayarathne, T., Kettler, J., Huang, Y., Thorne, P. S., O'Shaughnessy, P. T., and Stone, E. A.: Influence of rain on the abundance of bioaerosols in fine and coarse particles, Atmospheric Chemistry and Physics, 17, 2459–2475, https://doi.org/10.5194/acp-17-2459-2017, 2017.

Ren, G., Yan, X., Ma, Y., Qiao, L., Chen, Z., Xin, Y., Zhou, M., Shi, Y., Zheng, K., Zhu, S., Huang, C., and Li, L.: Characteristics and source apportionment of PM2.5-bound saccharides and carboxylic acids in Central Shanghai, China, Atmospheric Research, 237, 104 817, https://doi.org/10.1016/j.atmosres.2019.104817, 2020.

Ruske, S., Topping, D. O., Foot, V. E., Kaye, P. H., Stanley, W. R., Crawford, I., Morse, A. P., and Gallagher, M. W.: Evaluation of machine learning algorithms for classification of primary biological aerosol using a new UV-LIF spectrometer, Atmospheric Measurement Techniques, 10, 695–708, https://doi.org/10.5194/amt-10-695-2017, 2017.

Ruske, S., Topping, D. O., Foot, V. E., Morse, A. P., and Gallagher, M. W.: Machine learning for improved data analysis of biological aerosol using the WIBS, Atmospheric Measurement Techniques, 11, 6203–6230, https://doi.org/10.5194/amt-11-6203-2018, 2018.

Salter, M. E., Nilsson, E. D., Butcher, A., and Bilde, M.: On the seawater temperature dependence of the sea spray aerosol generated by a continuous plunging jet, Journal of Geophysical Research: Atmospheres, 119, 9052–9072, https://doi.org/10.1002/2013JD021376, 2014.

https://doi.org/10.5194/egusphere-2026-59
Preprint. Discussion started: 28 January 2026

Salter, M. E., Zieger, P., Acosta Navarro, J. C., Grythe, H., Kirkevåg, A., Rosati, B., Riipinen, I., and Nilsson, E. D.: An empirically derived inorganic sea spray source function incorporating sea surface temperature, Atmospheric Chemistry and Physics, 15, 11 047–11 066, https://doi.org/10.5194/acp-15-11047-2015, 2015.

Salter, M. E., Hamacher-Barth, E., Leck, C., Werner, J., Johnson, C. M., Riipinen, I., Nilsson, E. D., and Zieger, P.: Calcium enrichment in sea spray aerosol particles, Geophysical Research Letters, 43, 8277–8285, https://doi.org/10.1002/2016GL070275, 2016.

Sauvageat, E., Zeder, Y., Auderset, K., Calpini, B., Clot, B., Crouzy, B., Konzelmann, T., Lieberherr, G., Tummon, F., and Vasilatou, K.: Real-time pollen monitoring using digital holography, Atmospheric Measurement Techniques, 13, 1539–1550, https://doi.org/10.5194/amt-13-1539-2020, 2020.

Schiffer, J. M., Mael, L. E., Prather, K. A., Amaro, R. E., and Grassian, V. H.: Sea Spray Aerosol: Where Marine Biology Meets Atmospheric Chemistry, ACS Central Science, 4, 1617–1623, https://doi.org/10.1021/acscentsci.8b00674, pMID: 30648145, 2018.

Sikoparija, B., Matavulj, P., Simovic, I., Radisic, P., Brdar, S., Minic, V., Tesendic, D., Kadantsev, E., Palamarchuk, J., and Sofiev, M.: Classification accuracy and compatibility across devices of a new Rapid-E+ flow cytometer, Atmospheric Measurement Techniques, 17, 5051–5070, https://doi.org/10.5194/amt-17-5051-2024, 2024.

Simoneit, B. R. T.: A review of biomarker compounds as source indicators and tracers for air pollution, Environmental Science and Pollution Research, 6, 159–169, https://doi.org/10.1007/BF02987621, 1999.

Solomon, P. A., Fall, T., Salmon, L., Cass, G. R., Gray, H. A., and Davidson, A.: Chemical Characteristics of PM10 Aerosols Collected in the Los Angeles Area, JAPCA, 39, 154–163, https://doi.org/10.1080/08940630.1989.10466515, 1989.

Stone, E. A., Mampage, C. B. A., Hughes, D. D., and Jones, L. M.: Airborne sub-pollen particles from rupturing giant ragweed pollen, Aerobiologia, 37, 625–632, https://doi.org/10.1007/s10453-021-09702-x, 2021.

Su, B., Bi, X., Zhang, Z., Liang, Y., Song, C., Wang, T., Hu, Y., Li, L., Zhou, Z., Yan, J., Wang, X., and Zhang, G.: (Enrichment of calcium in sea spray aerosol: insights from bulk measurements and individual particle analysis during the R/V *Xuelong* cruise in the summertime in Ross Sea, Antarctica), Atmospheric Chemistry and Physics, 23, 10 697–10 711, https://doi.org/10.5194/acp-23-10697-2023, 2023.

Subba, T., Lawler, M. J., and Steiner, A. L.: Estimation of Possible Primary Biological Particle Emissions and Rupture Events at the Southern Great Plains ARM Site, Journal of Geophysical Research: Atmospheres, 126, e2021JD034 679, https://doi.org/10.1029/2021JD034679, e2021JD034679 2021JD034679, 2021.

Suphioglu, C., Singh, M., Taylor, P., Knox, R., Bellomo, R., Holmes, P., and Puy, R.: Mechanism of grass-pollen-induced asthma, The Lancet, 339, 569–572, https://doi.org/10.1016/0140-6736(92)90864-Y, originally published as Volume 1, Issue 8793, 1992.

Sánchez-Ochoa, A., Kasper-Giebl, A., Puxbaum, H., Gelencser, A., Legrand, M., and Pio, C.: Concentration of atmospheric cellulose: A proxy for plant debris across a west-east transect over Europe, Journal of Geophysical Research: Atmospheres, 112, https://doi.org/10.1029/2006JD008180, 2007.

Tang, D., Wei, T., Yuan, J., Xia, H., and Dou, X.: Observation of bioaerosol transport using wideband integrated bioaerosol sensor and coherent Doppler lidar, Atmospheric Measurement Techniques, 15, 2819–2838, https://doi.org/10.5194/amt-15-2819-2022, 2022.

Textor, C., Schulz, M., Guibert, S., Kinne, S., Balkanski, Y., Bauer, S., Berntsen, T., Berglen, T., Boucher, O., Chin, M., Dentener, F., Diehl, T., Easter, R., Feichter, H., Fillmore, D., Ghan, S., Ginoux, P., Gong, S., Grini, A., Hendricks, J., Horowitz, L., Huang, P., Isaksen, I., Iversen, I., Kloster, S., Koch, D., Kirkevåg, A., Kristjansson, J. E., Krol, M., Lauer, A., Lamarque, J. F., Liu, X., Montanaro, V., Myhre, G., Penner, J., Pitari, G., Reddy, S., Seland, Ø., Stier, P., Takemura, T., and Tie, X.: Analysis and quantification of the diversities of aerosol life cycles within AeroCom, Atmospheric Chemistry and Physics, 6, 1777–1813, https://doi.org/10.5194/acp-6-1777-2006, 2006.

https://doi.org/10.5194/egusphere-2026-59
Preprint. Discussion started: 28 January 2026

Tobo, Y., DeMott, P. J., Hill, T. C. J., Prenni, A. J., Swoboda-Colberg, N. G., Franc, G. D., and Kreidenweis, S. M.: Organic matter matters for ice nuclei of agricultural soil origin, Atmospheric Chemistry and Physics, 14, 8521–8531, https://doi.org/10.5194/acp-14-8521-2014, 2014.

Tobo, Y., Adachi, K., DeMott, P. J., Hill, T. C. J., Hamilton, D. S., Mahowald, N. M., Nagatsuka, N., Ohata, S., Uetake, J., Kondo, Y., and Koike, M.: Glacially sourced dust as a potentially significant source of ice nucleating particles, Nature Geoscience, 12, 253–258, https://doi.org/10.1038/s41561-019-0314-x, 2019.

Tobo, Y., Adachi, K., Kawai, K., Matsui, H., Ohata, S., Oshima, N., Kondo, Y., Hermansen, O., Uchida, M., Inoue, J., and Koike, M.: Surface warming in Svalbard may have led to increases in highly active ice-nucleating particles, Communications Earth & Environment, 5, 516, https://doi.org/10.1038/s43247-024-01677-0, 2024.

Toprak, E. and Schnaiter, M.: Fluorescent biological aerosol particles measured with the Waveband Integrated Bioaerosol Sensor WIBS-4: laboratory tests combined with a one year field study, Atmospheric Chemistry and Physics, 13, 225–243, https://doi.org/10.5194/acp-13-225-2013, 2013.

Venkateswara, H. and Panchanathan, S., eds.: Introduction to Domain Adaptation, pp. 3–21, Springer International Publishing, Cham, https://doi.org/10.1007/978-3-030-45529-3_1, 2020.

Vincenti, B., Paris, E., Carnevale, M., Palma, A., Guerriero, E., Borello, D., Paolini, V., and Gallucci, F.: Saccharides as Particulate Matter Tracers of Biomass Burning: A Review, International Journal of Environmental Research and Public Health, 19, https://doi.org/10.3390/ijerph19074387, 2022.

Visez, N., Chassard, G., Azarkan, N., Naas, O., Sénéchal, H., Sutra, J.-P., Poncet, P., and Choël, M.: Wind-induced mechanical rupture of birch pollen: Potential implications for allergen dispersal, Journal of Aerosol Science, 89, 77–84, https://doi.org/10.1016/j.jaerosci.2015.07.005, 2015.

Winiwarter, W., Bauer, H., Caseiro, A., and Puxbaum, H.: Quantifying emissions of primary biological aerosol particle mass in Europe, Atmospheric Environment, 43, 1403–1409, https://doi.org/10.1016/j.atmosenv.2008.01.037, natural and Biogenic Emissions of Environmentally Relevant Atmospheric Trace Constituents in Europe, 2009.

Wolf, M. J., Goodell, M., Dong, E., Dove, L. A., Zhang, C., Franco, L. J., Shen, C., Rutkowski, E. G., Narducci, D. N., Mullen, S., Babbin, A. R., and Cziczo, D. J.: A link between the ice nucleation activity and the biogeochemistry of seawater, Atmospheric Chemistry and Physics, 20, 15 341–15 356, https://doi.org/10.5194/acp-20-15341-2020, 2020.

Wozniak, M. C., Solmon, F., and Steiner, A. L.: Pollen Rupture and Its Impact on Precipitation in Clean Continental Conditions, Geophysical Research Letters, 45, 7156–7164, https://doi.org/10.1029/2018GL077692, 2018.

Xu, J., He, J., Xu, H., Ji, D., Snape, C., Yu, H., Jia, C., Wang, C., and Gao, J.: Simultaneous measurement of multiple organic tracers in fine aerosols from biomass burning and fungal spores by HPLC-MS/MS, RSC Adv., 8, 34 136–34 150, https://doi.org/10.1039/C8RA04991B, 2018.

Yttri, K. E.: ACTRIS, GAW-WDCA, EMEP, 2019-2021; Organic tracers at Zeppelin mountain (Ny-Ålesund), data hosted by EBAS at NILU, https://doi.org/10.48597/VYK3-XQEN, accessed 2025-6-16, 2023.

Yttri, K. E., Simpson, D., Nøjgaard, J. K., Kristensen, K., Genberg, J., Stenström, K., Swietlicki, E., Hillamo, R., Aurela, M., Bauer, H., Offenberg, J. H., Jaoui, M., Dye, C., Eckhardt, S., Burkhart, J. F., Stohl, A., and Glasius, M.: Source apportionment of the summer time carbonaceous aerosol at Nordic rural background sites, Atmospheric Chemistry and Physics, 11, 13 339–13 357, https://doi.org/10.5194/acp-11-13339-2011, 2011.

https://doi.org/10.5194/egusphere-2026-59
Preprint. Discussion started: 28 January 2026

Yttri, K. E., Schnelle-Kreis, J., Maenhaut, W., Abbaszade, G., Alves, C., Bjerke, A., Bonnier, N., Bossi, R., Claeys, M., Dye, C., Evtyugina, M., García-Gacio, D., Hillamo, R., Hoffer, A., Hyder, M., Iinuma, Y., Jaffrezo, J.-L., Kasper-Giebl, A., Kiss, G., López-Mahia, P. L., Pio, C., Piot, C., Ramirez-Santa-Cruz, C., Sciare, J., Teinilä, K., Vermeylen, R., Vicente, A., and Zimmermann, R.: An intercomparison study of analytical methods used for quantification of levoglucosan in ambient aerosol filter samples, Atmospheric Measurement Techniques, 8, 125–147, https://doi.org/10.5194/amt-8-125-2015, 2015.

Yttri, K. E., Bäcklund, A., Conen, F., Eckhardt, S., Evangeliou, N., Fiebig, M., Kasper-Giebl, A., Gold, A., Gundersen, H., Myhre, C. L., Platt, S. M., Simpson, D., Surratt, J. D., Szidat, S., Rauber, M., Tørseth, K., Ytre-Eide, M. A., Zhang, Z., and Aas, W.: Composition and sources of carbonaceous aerosol in the European Arctic at Zeppelin Observatory, Svalbard (2017 to 2020), Atmospheric Chemistry and Physics, 24, 2731–2758, https://doi.org/10.5194/acp-24-2731-2024, 2024.

Yu, X., Wang, Z., Zhang, M., Kuhn, U., Xie, Z., Cheng, Y., Pöschl, U., and Su, H.: Ambient measurement of fluorescent aerosol particles with a WIBS in the Yangtze River Delta of China: potential impacts of combustion-related aerosol particles, Atmospheric Chemistry and Physics, 16, 11 337–11 348, https://doi.org/10.5194/acp-16-11337-2016, 2016.

Zangrando, R., Barbaro, E., Kirchgeorg, T., Vecchiato, M., Scalabrin, E., Radaelli, M., Đorđević, D., Barbante, C., and Gambaro, A.: Five primary sources of organic aerosols in the urban atmosphere of Belgrade (Serbia), Science of The Total Environment, 571, 1441–1453, https://doi.org/10.1016/j.scitotenv.2016.06.188, 2016.

Zhang, H., Zheng, X., Xie, N., He, Z., Liu, J., Leung, N. L. C., Niu, Y., Huang, X., Wong, K. S., Kwok, R. T. K., Sung, H. H. Y., Williams, I. D., Qin, A., Lam, J. W. Y., and Tang, B. Z.: Why Do Simple Molecules with "Isolated" Phenyl Rings Emit Visible Light?, Journal of the American Chemical Society, 139, 16 264–16 272, https://doi.org/10.1021/jacs.7b08592, 2017.

Zhang, H., Crawford, I., Song, C., Gallagher, M., Zheng, Z., Chan, M. N., Xing, S., Lee, H. B. M., and Topping, D.: Data-Driven Detection of Nocturnal Pollen Fragmentation Triggered by High Humidity in an Urban Environment, Environmental Science & Technology, 59, 12 763–12 774, https://doi.org/10.1021/acs.est.4c13905, 2025.

Zimmermann, B.: Characterization of Pollen by Vibrational Spectroscopy, Applied Spectroscopy, 64, 1364–1373, https://doi.org/10.1366/000370210793561664, pMID: 21144154, 2010.

Zinke, J., Pereira Freitas, G., Foster, R. A., Zieger, P., Nilsson, E. D., Markuszewski, P., and Salter, M. E.: Quantification and characterization of primary biological aerosol particles and microbes aerosolized from Baltic seawater, Atmospheric Chemistry and Physics, 24, 13 413–13 428, https://doi.org/10.5194/acp-24-13413-2024, 2024.

https://doi.org/10.5194/egusphere-2026-59
Preprint. Discussion started: 28 January 2026

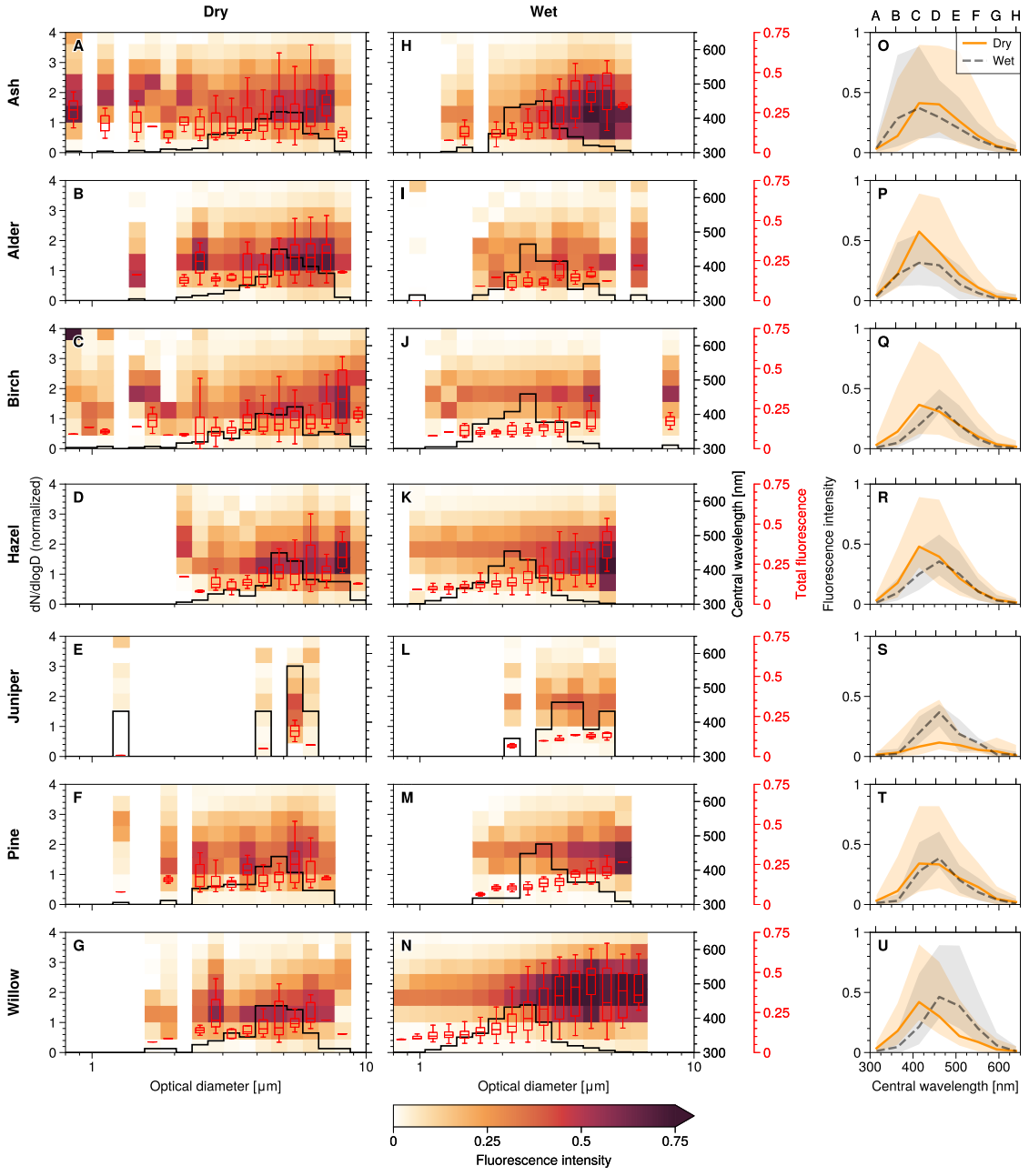

Figure 1. Pollen fluorescence properties and size distributions measured in our characterization experiments. Size distributions (left axis, black step trace) and fluorescence emission spectra (right axis, color map) for highly fluorescent particles (HFPs) with $> 9\sigma$ fluorescence signal, binned by size, in (a-g) dry and (h-n) wet pollen characterization experiments. Box plots (red axes) depict the range of total fluorescence in each size bin. Fluorescence intensities are given as a fraction of detector maxima at saturation. (o-u): The median fluorescence emission spectra of HFPs in dry (solid) and wet (dashed) pollen experiments at all sizes; shaded areas represent 10-90% quantile ranges. Upper axes show fluorescence detection channel names corresponding to their central detection wavelengths in the lower axes.

https://doi.org/10.5194/egusphere-2026-59
Preprint. Discussion started: 28 January 2026

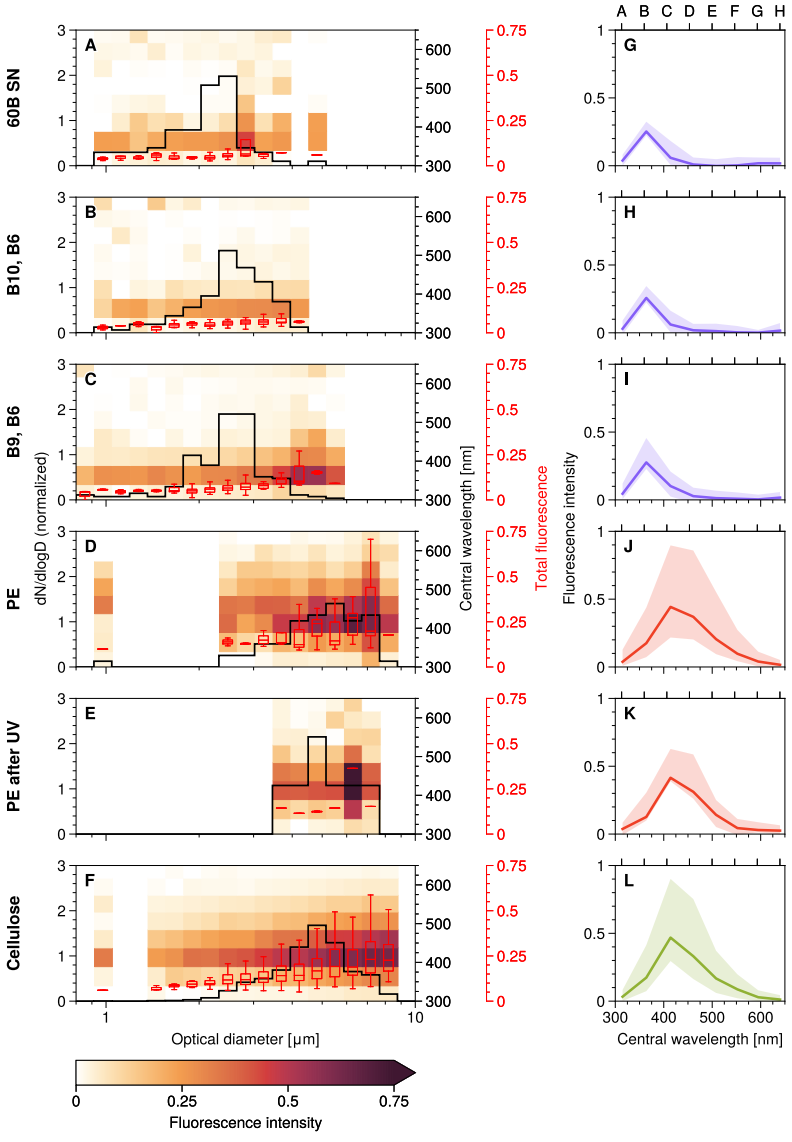

Figure 2. Bacteria, microplastic, and cellulose fluorescence properties and size distributions measured in our characterization experiments. (a-f) show size distributions (left axis, black step trace) and fluorescence emission spectra (right axis, color map) for highly fluorescent particles (HFPs) with $> 9\sigma$ fluorescence signal, binned by size, for bacteria (a-c), fresh and UV-aged polyethylene (PE) (d-e, respectively), and cellulose (f). Box plots (red axes) depict the range of total fluorescence in each size bin. Fluorescence intensities are given as a fraction of detector maxima at saturation. (o-u) show the median fluorescence emission spectra of HFPs at all sizes for these experiments; shaded areas represent 10-90% quantiles. Upper axes show fluorescence detection channel names corresponding to their central detection wavelengths in the lower axes.

https://doi.org/10.5194/egusphere-2026-59
Preprint. Discussion started: 28 January 2026

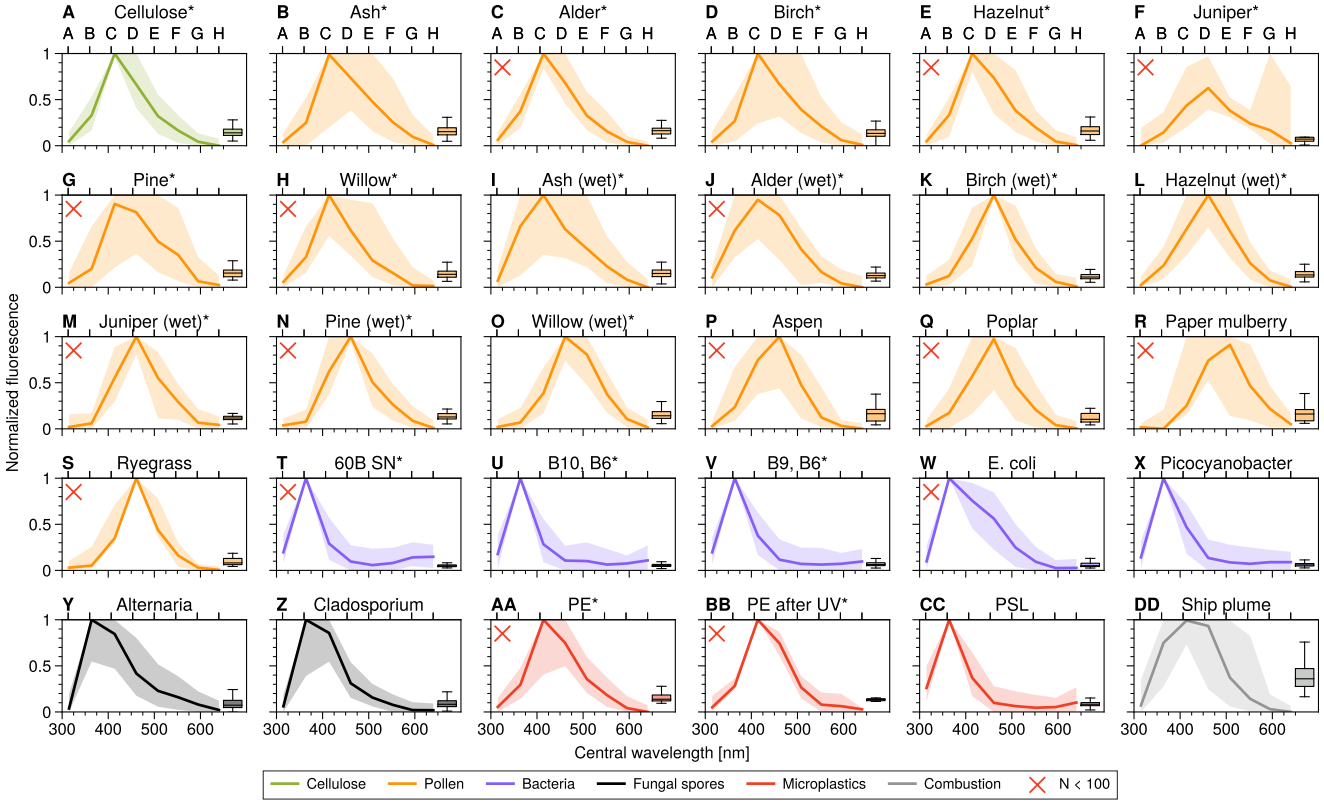

Figure 3. Fluorescence emission spectra (normalized by the maximum fluorescence signal measured for each particle) for particles with $> 9\sigma$ fluorescence signal for all source experiments. Shaded regions indicate 10-90% quantile ranges. Box plots indicate the distribution of total fluorescence (normalized by the maximum possible signal) among particles. Source experiments conducted in this study are marked with an asterisk. Experiments with a sample size of <100 are marked with an X in the subplot.

https://doi.org/10.5194/egusphere-2026-59
Preprint. Discussion started: 28 January 2026

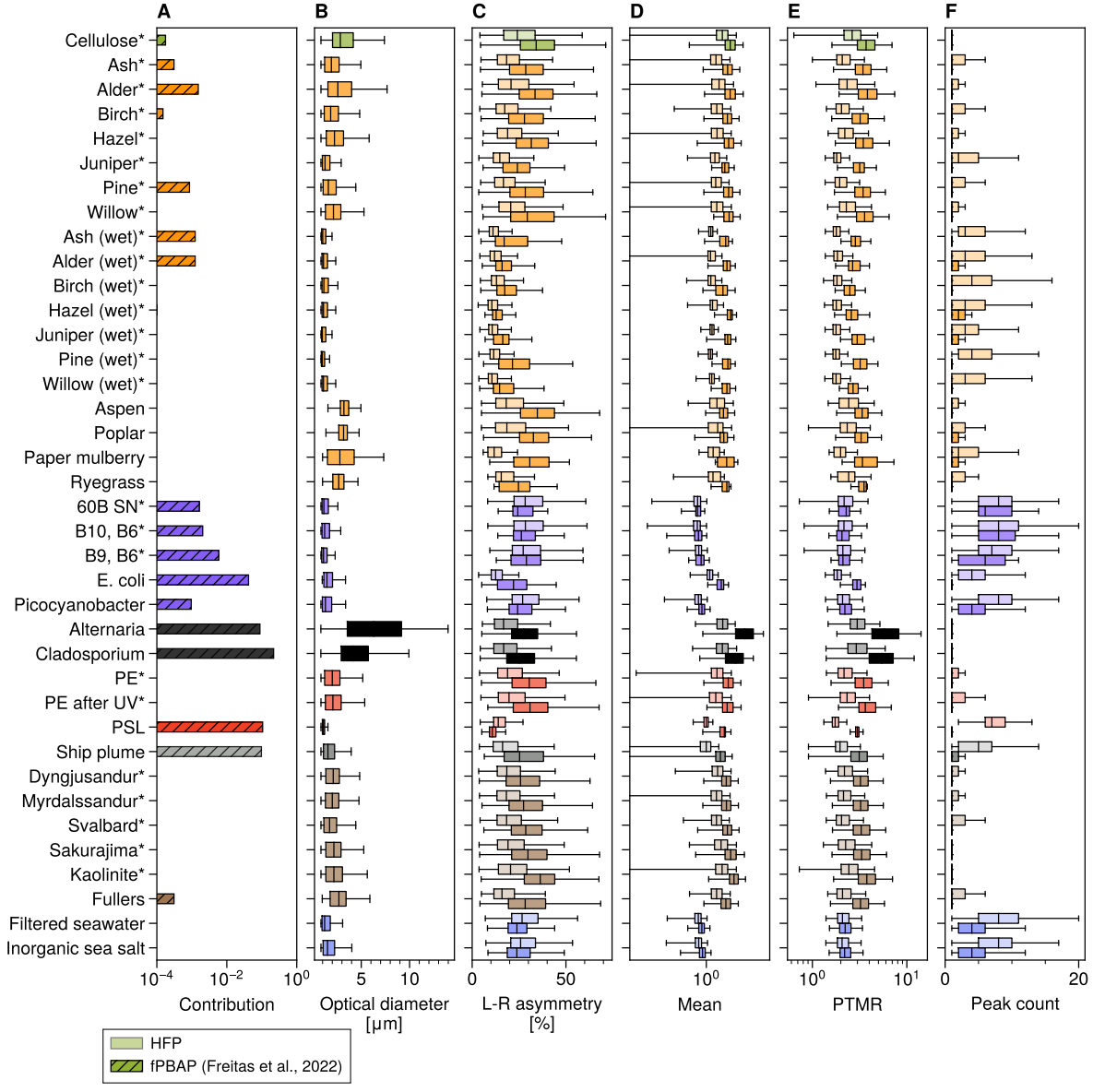

Figure 4. Comparison of particle property distributions for all source data. (a): Contributions to total particles measured in the samples by highly fluorescent particles (HFPs) and fluorescent primary biological aerosol particles (fPBAPs) as identified by the decision tree method of Freitas et al. (2022). For the ship plume, only HFPs are displayed. (b-f): Size (b) and morphology parameters (c-f) of particles in the samples. In (c-f), dark (light) boxes indicate $<$ ($\geq$) 3 µm particles. The right array is shown for single-array morphology parameters (d-f).

https://doi.org/10.5194/egusphere-2026-59
Preprint. Discussion started: 28 January 2026

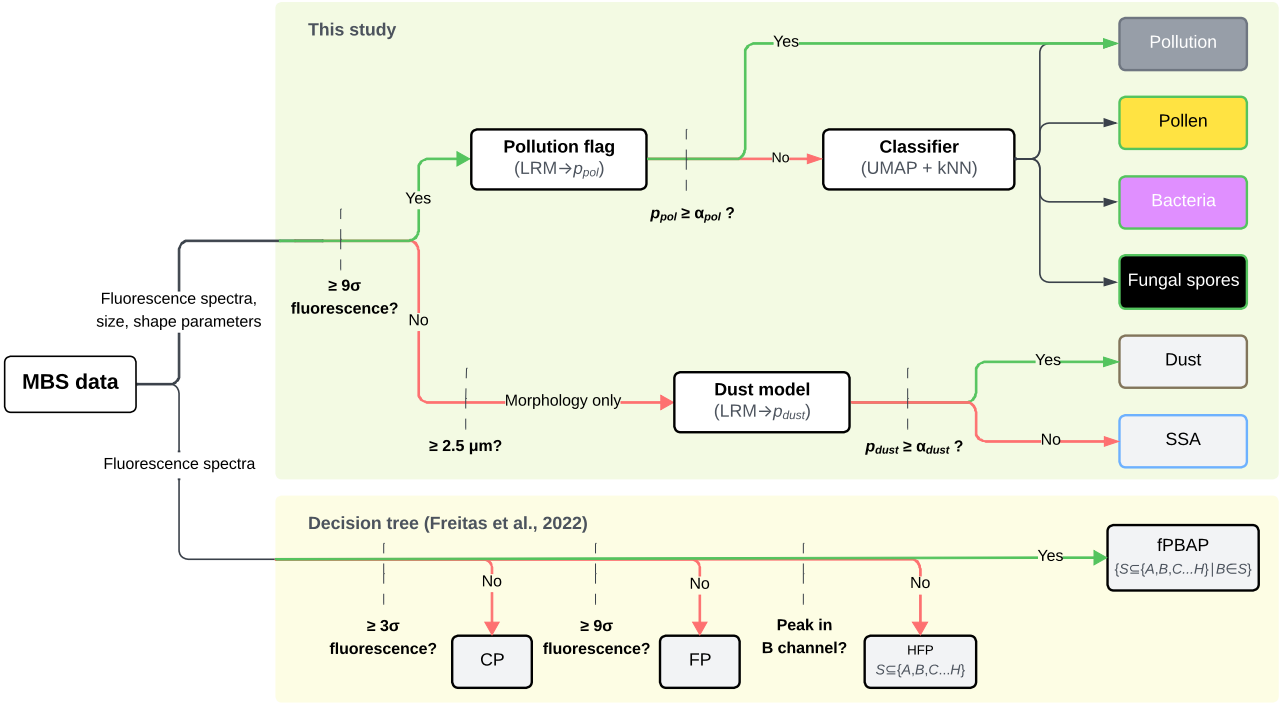

Figure 5. A schematic illustrating the particle classification schemes of this study (top branch) and of Freitas et al. (2022) (bottom branch). Dashed lines represent filtering and decision-based steps. In the pollution and dust logistic regression models (LRMs), p is the output probabilities for being flagged as pollution or dust, respectively, and α represents a chosen confidence level. The bioaerosol classifier using uniform manifold approximation and projection (UMAP) and k-nearest neighbors (kNN) classify according to the most likely class. Among highly fluorescent particles (HFPs) and fluorescent biological aerosol particle (fPBAP) classes in the decision tree-based method of Freitas et al. (2022) (lower branch), the class label is denoted as S and consists of combinations of letters A through H corresponding to the fluorescence channels where significant ($> 9\sigma$) fluorescence is detected. According to the fPBAP definition, all fPBAP class labels contain B. Specific information about the exact variables used as input for each method is found in the text.

https://doi.org/10.5194/egusphere-2026-59
Preprint. Discussion started: 28 January 2026

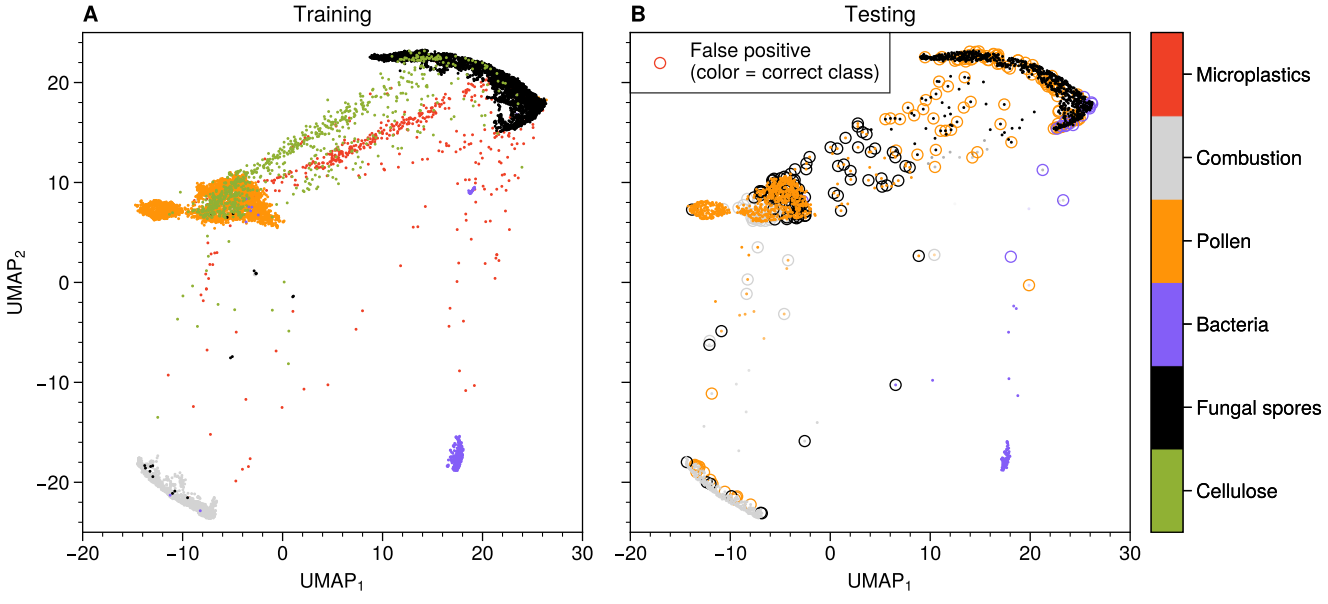

Figure 6. Uniform manifold approximation and projection (UMAP) phase space locations of particles for (a) training and (b) testing data. Note that the UMAP approximator and k-nearest neighbors (kNN) models are trained only with combustion, pollen, bacteria, and fungal spore data and not with microplastics and cellulose classes. In (a), the color coding for markers is according to the known particle class. In (b), the marker color is according to the kNN-predicted class, and the alpha of the marker denotes the confidence of the prediction; misclassifications are circled, with the circle's color denoting the correct class.

https://doi.org/10.5194/egusphere-2026-59
Preprint. Discussion started: 28 January 2026

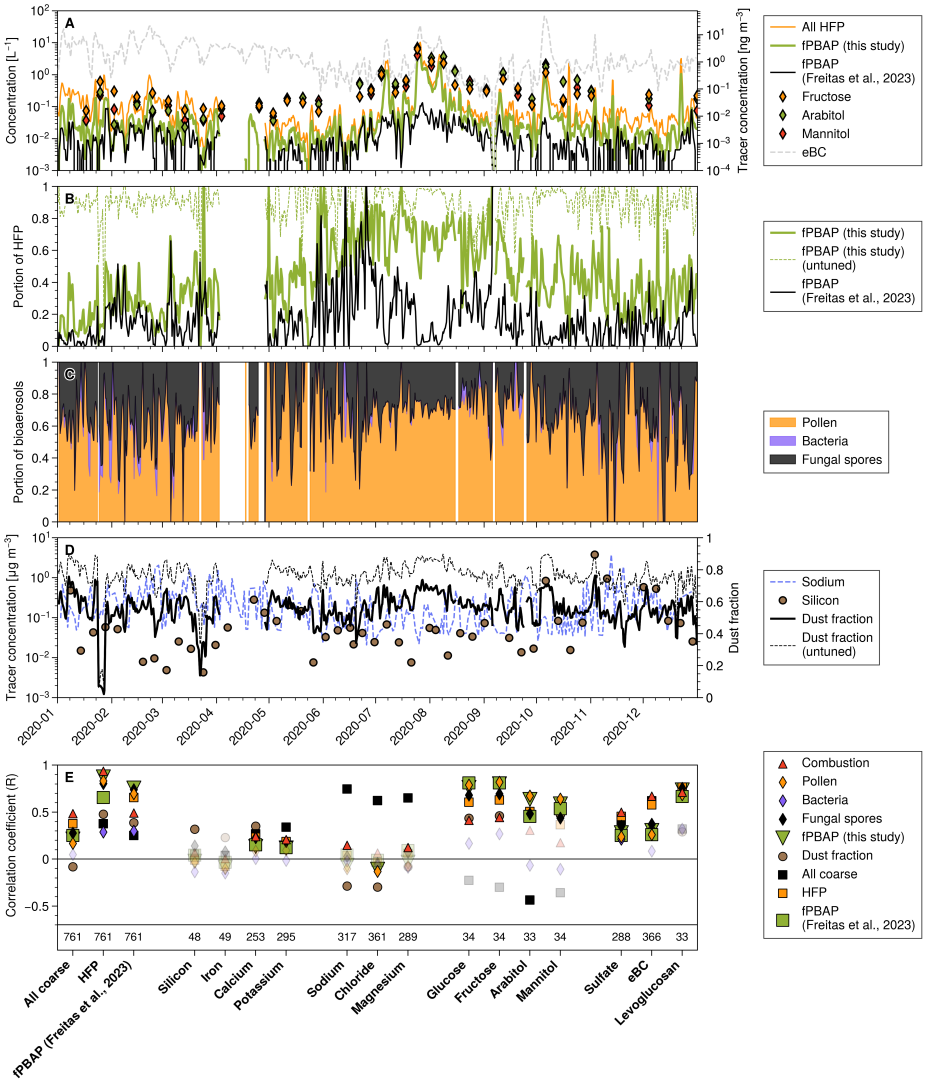

Figure 7. Algorithm performance using field observations made at Zeppelin Observatory, Svalbard during 2020. (a) Left axis: time series of highly fluorescent particle (HFP) and fluorescent primary biological aerosol particle (fPBAP) concentrations according to our classifier (this study) and using the decision tree (DT)-based method of Freitas et al. (2023a). Right axis: concentrations of biological tracers fructose, arabitol, and mannitol, and combustion tracer equivalent black carbon (eBC). (b) Contributions to all HFP by fPBAP using our classifier (both tuned and untuned) and the DT method. (c) Contributions by individual fPBAP classes (pollen, bacteria, and fungal spores) to fPBAP concentrations. (d) Time series for sodium and silicon concentrations (left axis) and the fraction of particles $\geq$2.5 µm identified as dust (both tuned and untuned) (right axis). (e) Spearman correlation coefficients between concentrations for all coarse particles, HFPs, fPBAP (determined using both our algorithm and the DT method), individual fPBAP classes identified by our algorithm, and chemical tracers. Correlations not significant with $p < 0.05$ are made transparent. Tracers used in the domain adaptation steps are marked with an asterisk. The bottom panel displays sample sizes for each tracer.